CANADIAN SPACE AGENCY
Earth Observation Applications Development
Program (EOADP)

Canadian Space Agency
Agence spatiale canadienne

Report Documentation Page

Report #: IMP_RP_53_8863_001_MDA_9F043120631_10Mar2016	**Report Date:** March 10, 2016
Title: EOADP InSAR for Monitoring Permafrost Final Report	
Author(s): Jayson Eppler, Mike Kubanski and Jennifer Busler	
Performing Organisation(s) Name and Address(es): MDA Systems Ltd. 13800 Commerce Parkway Richmond, BC, Canada V6V 2J3 Tel: (604) 278-3411 Fax: (604) 231-2753 Project Manager: Jennifer Busler	**Performing Organisation Report #:** IMP-RP-53-8865
Sponsoring Agency Name(s)and Address(es): Canadian Space Agency 6767 Route de l'Aeroport Saint-Hubert, Quebec J3Y 8Y9 Tel: (450) 926-4800 Fax: (450) 926-4613 Technical Authority: Corey Froese Program Authority: Lyse Champagne	**CSA Contract #:** #9F043-120631/002/MTB InSAR for Monitoring Permafrost

Abstract:
Under the InSAR for Monitoring Permafrost EOADP, we aim to provide an InSAR based solution using data from RADARSAT-2 and potentially other SAR satellites to assist governments and transportation agencies plan, develop and maintain transportation related infrastructure in permafrost affected areas. The project objective is to develop and demonstrate an InSAR based deformation monitoring solution focused on infrastructure in permafrost affected areas using C- and X-band SAR imaging systems. This document provides a technical summary of the work performed, results and project evaluation.

Key Words:
RADARSAT-2, TerraSAR-X, COSMO-SkyMed, Interferometric SAR, Permafrost, Infrastructure

Supplementary Notes:

THIS PAGE INTENTIONALLY LEFT BLANK

EOADP InSAR for Monitoring Permafrost (IMP)

Final Report

CSA Contract No: 9F043-120631/002/MTB

Prepared By: Jayson Eppler

Prepared By: Mike Kubanski

Project Manager: Jennifer Busler

Released by CADM: Jan Chappell

CADM signature indicates that all above approvals have been received and are on file.

13800 Commerce Parkway
Richmond, B.C., Canada, V6V 2J3
Telephone (604) 278-3411
Fax (604) 278-2117

CHANGE RECORD

ISSUE	DATE	PAGE(S)	DESCRIPTION
1/0	Mar. 10, 2016	All	First Issue

TABLE OF CONTENTS

LIST OF FIGURES

LIST OF TABLES

ACRONYMS AND ABBREVIATIONS

AO	Announcement of Opportunity
BIP	Background Intellectual Property
CEN	Centre d'Études Nordique
CEOS	Committee on Earth Observation Satellites
CR	Corner Reflector
CSA	Canadian Space Agency
CSK	COSMO-SkyMed
DAP	Data Acquisition Plan
DEM	Digital Elevation Model
DInSAR	Differential InSAR
EOADP	Earth Observation Application Development Program
ENVISAT	ENVIronmental SATellite
EQA	Equiangular coordinates
FIP	Foreground Intellectual Property
GAMMA	InSAR Processing Software from GAMMA Remote Sensing
GDAL	Geospatial Data Abstraction Library
GeoTIFF	Geographic Tagged Image File Format
HDS	Homogeneous Distributed Scatterer
IEEE	Institute of Electrical and Electronics Engineers
IGARSS	Geoscience and Remote Sensing Symposium
IMP	InSAR for Monitoring Permafrost
InSAR	Interferometric Synthetic Aperture Radar
IP	Intellectual Property
ISRSE	International Symposium on Remote Sensing of Environment
MDA	MDA Systems Ltd.
MF	Multi-Look Fine
NMSO	National Master Standing Offer
RDC	Range Doppler Coordinates
RHEL	Red Hat Enterprise Linux
RS-2	RADARSAT-2
SVD	Singular Value Decomposition

TC	Transport Canada
TSX	TerraSAR-X (radar satellite)
YHPW	Yukon Highways and Public Works
UTM	Universal Transverse Mercator

1 EXECUTIVE SUMMARY

Background and Objectives

This project aims to develop an InSAR based solution using data from RADARSAT-2 and potentially other SAR satellites to assist governments and transportation agencies plan, develop and maintain transportation related infrastructure in permafrost affected areas. The project objective is to develop and demonstrate an InSAR based deformation monitoring solution focused on infrastructure in permafrost affected areas using C- and X-band SAR imaging systems.

To develop and demonstrate a solution that addressed these objectives multiple test sites were required to capture representative examples of both infrastructure and local permafrost and surficial conditions. Umiujaq, Salluit, Beaver Creek and Inuvik were selected as test sites, where a combination of RADARSAT-2, TerraSAR-X and COSMO-SkyMed datasets over these sites were collected from January 2013 to November 2015. Additionally a set of archive data datasets over Yellowknife were obtained and used as a test dataset prior to accumulation of data over the other sites.

Results and Conclusions

The key outcome of this project has been the development of an InSAR solution that specifically addresses challenges faced by monitoring permafrost affected areas. This solution is based on MDA's Multi-Track HDS-InSAR technique that is able to jointly process one or more same side SAR datasets from potentially multiple satellites to estimate deformation time series for both point-like and spatially distributed coherent targets. The developed solution includes a model for seasonal active layer deformation which allows for estimation of long-term linear deformation trends over a relatively short time period and optionally allows for use of winter SAR acquisitions to quantify the full seasonal displacement affecting areas with an ice-rich active layer.

InSAR products generated from applying MDA's solution to image data collected over our test sites at Umiujaq, Salluit, Beaver Creek and Yellowknife have shown that the method provides deformation estimates at a high spatial point coverage for most surficial conditions. Prior to the start of the project MDA's InSAR solution required at least two years of data to generate surface deformation time series estimates. The Multi-Track HDS-InSAR solution is now able to generate time series estimates from a single summer season if multiple concurrent datasets are processed. Furthermore, the method allows for the separation of seasonal and linear deformation components over time periods as short as 2 years. A comparison of deformation results with surficial geology conditions show the expected strong correlation between surficial geology and the distribution of surface deformation and demonstrates that the InSAR results provide complimentary information to that provided using only surficial geology maps.

A comparison of results from applying the solution using both C- and X-band data both individually and in combination shows very similar spatial coherent target coverage and deformation estimates. This confirms that the solution can be effectively applied for monitoring permafrost affected areas with either C- or X-band data. However it should be noted that more frequent data acquisitions are required for X-band compared to C-band due to higher rates of temporal decorrelation present in X-band datasets.

2 DOCUMENTS

2.1 Applicable Documents

A-1	9F043-120631/002/MTB	Advanced EO Products & Services. Contract Issued 29 May 2013 and all amendments. PWGSC.
A-2	01-7697	Use of RADARSAT-based InSAR for Permafrost Infrastructure Monitoring in the Canadian North. Proposal submitted March 2013. MDA.
A-3	IMP-MN-53-5423	IMP Kick-off Meeting Minutes. Released 31 July 2013. MDA.

2.2 Reference Documents

R-1	IMP-PL-53-5750	IMP Data Acquisition Plan. Issue 2/0. May 2014. MDA.
R-2	IMP-RP-53-5775	IMP Milestone Report #1. Issue 1/0. October 2013. MDA.
R-3	IMP-RP-53-6672	IMP Milestone Report #2. Issue 1/0. May 2014. MDA.
R-4	IMP-RP-53-7286	IMP Milestone Report #3. Issue 1/0. December 2014. MDA.
R-5	IMP-RP-53-8035	IMP Milestone Report #4. Issue 1/0. May 2015. MDA.
R-6	IMP-RP-53-8769	IMP Milestone Report #5. Issue 1/0. December 2015. MDA.
R-7		Liu, Lin, et al. "Estimating 1992–2000 average active layer thickness on the Alaskan North Slope from remotely sensed surface subsidence." Journal of Geophysical Research: Earth Surface (2003–2012) 117.F1 (2012).
R-8		Wolfe, S A; Kerr, D E, Geological Survey of Canada, Canadian Geoscience Map 183, 2014; 1 sheet, doi:10.4095/293725

R-9 Wolfe, Stephen A., et al. "Evaluation of RADARSAT-2 DInSAR seasonal surface displacement in discontinuous permafrost terrain, Yellowknife, Northwest Territories, Canada." Canadian Journal of Remote Sensing 40.6 (2014): 406-422.

R-10 Seto, J. T. C., et al. "Investigation and assessment of runways overlying warm permafrost, Yellowknife airport." Proceedings of the 12th International Specialty Conference on Cold Regions Engineering, Canadian Society of Civil Engineering, Edmonton, Alberta, Canada. 2004.

R-11 Beck, I., et al. "Vertical movements of frost mounds in subarctic permafrost regions analyzed using geodetic survey and satellite interferometry." Earth Surface Dynamics 3.3 (2015): 409.

R-12 Goel, Kanika, and Nico Adam. "High resolution differential interferometric stacking via adaptive spatial phase filtering." Geoscience and Remote Sensing Symposium (IGARSS), 2011 IEEE International. IEEE, 2011.

3 INTRODUCTION

3.1 Purpose

The Interferometric Synthetic Aperture Radar (InSAR) for Monitoring Permafrost (IMP) project is funded by the Canadian Space Agency (CSA) through their Earth Observation Application Development Program (EOADP) to develop applications using advanced earth observation techniques for Government of Canada end-user agencies (Contract No. 9F043-120631/002/MTB) [A-1]. Transport Canada (TC) is identified as our Government of Canada end-user. However, as infrastructure falls under the responsibility of federal, territorial and municipal governments, representatives from the Yukon department of Highways and Public Works and Northwest Territories Department of Transportation are also engaged as participants in the project [A-3].

The technical objectives of this project are to demonstrate to Transport Canada and their partners novel InSAR deformation analysis methods that are tailored to monitor the effects of permafrost on infrastructure in the Canadian North [A-1], including:

- Mapping and monitoring existing infrastructure displacement and areas of risk in permafrost regions.
- Identification of ice-rich and unstable areas of permafrost for infrastructure planning.
- Evaluating the effectiveness of Advanced InSAR methods in characterizing permafrost deformation patterns and remediation techniques in maintaining infrastructure stability in permafrost regions, where possible.

For this work, MDA Systems Ltd. (MDA) has partnered with Prof. Michel Allard's team at Université Laval Centre d'Études Nordiques (CEN) who provide expertise in permafrost research and in-situ data from their field sites.

3.2 Scope

This document describes MDA's solution for InSAR based monitoring of infrastructure in permafrost areas using satellite based SAR imagery. This process required:

1. Acquiring satellite based SAR imagery used to conduct the InSAR analysis.
2. Building on MDA's existing InSAR solution through implementation of new advanced InSAR algorithms and tools to address specific challenges posed by monitoring in permafrost affected areas.
3. Generating deformation products and co-analyzing these with ancillary data for the interpretation of the results.
4. Evaluation of system performance using both C- and X-band SAR data individually and in combination.

5. An investigation of alternate data sampling scenarios (different spatial resolutions and temporal sampling strategies) in order to identify cost effective monitoring strategies

Each of the steps is discussed in this report.

3.3 Document Structure

This document is structured as follows:

- Section 4 describes the input data.
- Section 5 discusses the InSAR algorithm development.
- Section 6 presents InSAR deformation monitoring results over the study sites.
- Section 7 presents a comparative C-/X-band analysis.
- Section 8 present results from alternate dataset processing scenarios.
- Section 9 describes project conclusions and recommendations.
- Appendix A describes developed and delivered software tools.

3.4 Target Audience

This document is intended for the IMP project team at MDA Systems Ltd. and the CSA. The document contains information proprietary to MDA that shall not be communicated publically.

4 DATA ACQUISITION

SAR data acquisition for the project included RADARSAT-2, TerraSAR-X and COSMO-SkyMed images and covered five sites: Beaver Creek, YK (Yukon-Alaska Highway, YK), the Inuvik-to-Tuktoyaktuk Highway (NT), Yellowknife (NT) Salluit (QC) and Umiujaq (QC). All acquisitions were completed by November 2015.

Table 4-1 provides of a summary of the test sites including InSAR stacks, available ancillary data, and beam footprints. Note that the term 'stack' refers to a time-series set of spatially coincident SAR images collected using the same imaging geometry. A full description of the SAR image, ground measurement, and ancillary data needs for the IMP project, including a description and justification of data to be acquired for each of the proposed study sites is available in the Data Acquisition Plan (DAP) [R-1], which remains unchanged from the previous reporting period.

Table 4-1 IMP Study Sites Summary

Site	InSAR stacks	Summary/Ancillary Data	Beam Footprints
Yellowknife	RADARSAT-2 2xUltrafine	Site to be used for algorithm development with two thick RADARSAT-2 archive stacks. Allows for the development and testing of new methods to commence early without having to wait for suitable stacks to be acquired. No ground measurements are planned, although CCRS publications and GIS layers from the NT government will aid in the interpretation of results.	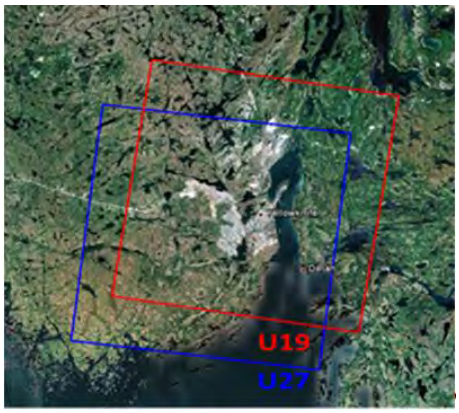
Umiujaq	RADARSAT-2 3xSpotlight 1xUltrafine TerraSAR-X 1x High-Res Spotlight 2x Staring Spotlight COSMO-SkyMed	Three spotlight scenes are selected to perform multi-stack processing at the best spatial resolution available. An additional ultrafine stack is added to acquire a wider margin of surrounding terrain. Three TSX stacks are acquired for an X-/C-band comparison study. One CSK stack with short revisit times is acquired to capture seasonal permafrost dynamics over one summer. Anchored and floating corner reflectors (CRs) are installed at this site.	RADARSAT-2:

Site	InSAR stacks	Summary/Ancillary Data	Beam Footprints
	1x Spotlight		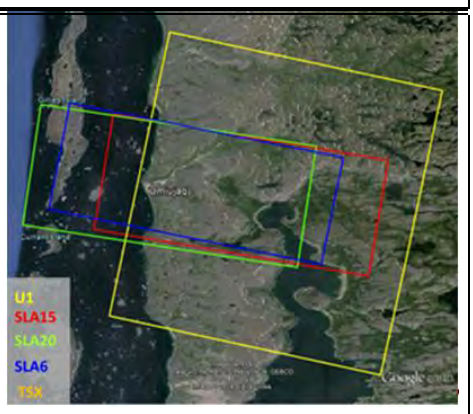
	7 CRs	Rich ancillary data is available from CEN including meteorological station data, thermistor cable data, surficial geology maps, and additional ground measurements.	TerraSAR-X:  COSMO-SkyMed: 

Site	InSAR stacks	Summary/Ancillary Data	Beam Footprints
Salluit	RADARSAT-2 1xSpotlight TerraSAR-X 1x High-Res Spotlight 2x Staring Spotlight	This is an important in-situ monitoring site for CEN, containing their permafrost infrastructure testbed. Due to significant conflicts a single RADARSAT-2 spotlight beam (with ongoing conflicts) is ordered. Three TSX stacks are also acquired over this site to allow an InSAR evaluation of the infrastructure testbed. CEN has installed significant instrumentation at this site including automated and manual meteorological stations, thermistor cables, and distributed temperature sensing measurements.	
Inuvik-to-Tuktoyaktuk Highway	RADARSAT-2 3xUltrafine	This proposed highway is an important piece of infrastructure and represents an extended footprint to monitor. The southern end of the route was selected because it also provides the opportunity to monitor the significant infrastructure within the town of Inuvik. Ultrafine beams were chosen because they provide a good compromise between spatial resolution and coverage footprint. The three beams will be used for InSAR multi-stack processing. Additional ongoing stacks over Tuktoyaktuk are available if the ITH becomes a priority. Ancillary data available for this site include a high-resolution DEM, optical imagery, and GIS layers provided by the NT Centre of Geomatics and Municipal and Community Affairs.	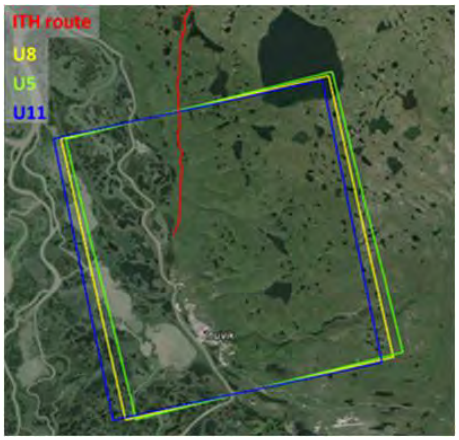
Alaska Highway	RADARSAT-2 1xMultilook Fine 3xSpotlight TerraSAR-X 1x Staring Spotlight	This existing and heavily-used highway represents an extended footprint to monitor. Due to the concentration of permafrost remedial measures being tested as well as strong permafrost degradation over the surrounding area, acquisitions are focused on the Beaver Creek site. Three RADARSAT-2 and one TSX spotlight stacks will provide high-resolution coverage of the testbed and one Multi-Look fine stack will give coverage over a wider area to the Alaska border. Additional background acquisitions over other portions of the highway are available if desired. Ancillary data from the YGS includes geotechnical borehole data, weather stations, ground temperatures, and permafrost thickness. Geophysical survey data along the highway is available from YHPW.	

A summary count of the RADARSAT-2, TerraSAR-X and COSMO-SkyMed images received are given in Table 4-2, Table 4-3 and Table 4-4 respectively. Note that 'Missing' is used to identify gaps within prospectively acquired data orders and do not apply to orders placed out of the RADARSAT-2 data archive.

Table 4-2 RADARSAT 2 Image Acquisition Status for IMP Sites

Site	Mode	Received	Pending	Missing/Failed	Total
Yellowknife, NT	U19	26	0	0	26
	U27	33	0	0	33
Umiujaq, QC	U1	31	0	6	37
	SLA15	39	0	1	40
	SLA20	36	0	1	37
	SLA6	34	0	2	36
Salluit, QC	SLA1	31	0	9	40
Inuvik, NT	U11	34	0	3	37
	U8	32	0	4	36
	U5	36	0	0	36
Alaska Highway, YT	MF22N	36	0	0	36
	SLA12	36	0	1	37
	SLA16	36	0	0	36
	SLA20	34	0	2	36

Table 4-3 TerraSAR-X Image Acquisition Status for IMP Sites

Site	Mode	Acquired	Pending	Missing/Failed	Total
Umiujaq, QC	HS spot24	45	0	3	48
	ST spot27	23	0	4	27
	ST spot75	26	0	3	29
Salluit, QC	HS spot39	46	0	1	47
	ST spot17	45	0	3	48
	ST spot60	26	0	4	30
Alaska Highway, YT	ST spot34	25	0	7	32

Table 4-4 COSMO-SkyMed Image Acquisition Status for IMP Sites

Site	Mode	Acquired	Pending	Missing/Failed	Total
Umiujaq, QC	SL12	20	0	0	20

Site visits to install, inspect and maintain the corner reflector installation at Umiujaq and take site photos of areas of interest at Umiujaq and Salluit were carried out regularly throughout the project with visits taking place in October 2013, June 2014, October 2014, April 2015, June 2015 and September 2015.

5 INSAR METHODS NEW DEVELOPMENT & TESTING

A solution for InSAR monitoring of permafrost affected area must address several unique challenges. These include:

- Extended snow cover season significantly reduces the number of viable interferograms that do not suffer severe snow related decorrelation
- Dry snow biases phase in winter-winter interferograms
- Complex deformation dynamics superimpose long term and seasonal deformation components
- Ice content and corresponding surface expression may be highly spatially variable leading to spatial phase gradients affecting unwrapping performance

The IMP project included tasks for the development of new methods to complement MDA's existing InSAR solution in order to address these specific challenges. This section provides an overview of the various solution components that were developed and tested during the project.

5.1 Hard target atmospheric screens algorithm

The goal of this task was to address the effects of snow related phase bias. Dry snow has the effect of biasing the interferometric phase without destroying coherence. Hence interferograms spanned by winter scenes can often contain extensive coherent areas but be biased by this additional phase term for any targets covered by dry snow. Since this phase component is generally spatially wide in scale it tends to influence the computed long scale atmospheric phase screens. This creates a problem for those targets not biased by dry snow such as snow free structural elements on buildings and other infrastructure since the long scale phase screens are subtracted from all targets during InSAR processing.

Work was done to implement a modified approach for atmospheric screen estimation to address this issue. The approach taken was to use the spectral coherence magnitude computed over all SAR acquisitions to identify those targets with minimal geometric speckle. These targets are assumed to be more point-like throughout all seasons compared to other targets and are less likely to be snow covered. These so called 'hard targets' were then used to construct nominally snow-free atmospheric phase screens.

The effectiveness of this method was tested by comparing the temporal coherence of all hard targets processed with the standard 'all target' atmospheric screens and also the hard-target atmospheric screens. The method resulting in higher temporal coherence magnitudes can be considered the preferred screen generation method since it results in the least biased phase for hard targets.

Figure 5-1 shows the distribution of hard target temporal coherence magnitude using the two methods. This clearly shows that the standard APS results in higher coherence values. All InSAR processing for the project was therefore performed using the standard APS method rather than the hard targets APS algorithm.

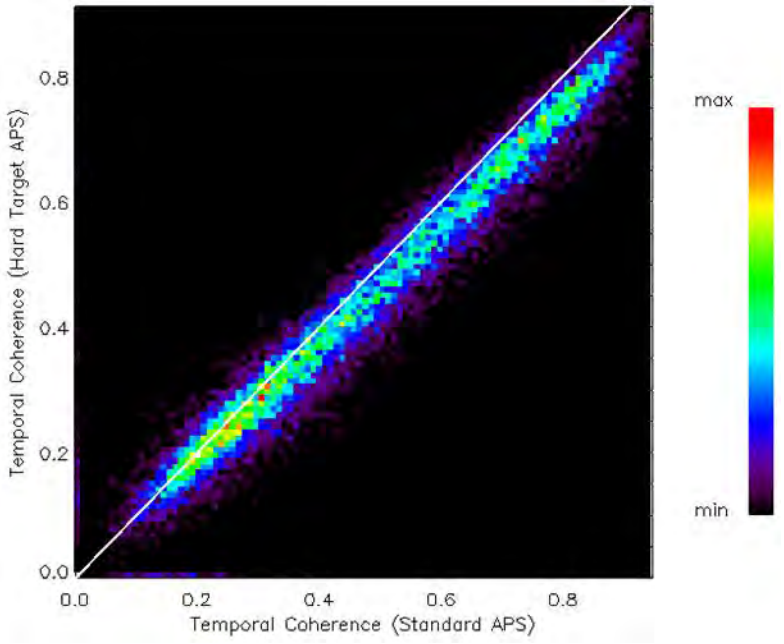

Figure 5-1 2D histogram of absolute temporal coherence for hard targets de-biased using hard-target phase screens vs. standard phase screens.

5.2 High Temporal Resolution HDS-InSAR method

Several enhancements to the Multi-Track HDS InSAR (MTI) solution were made during the project. It should be noted that this solution has also been referred to as 'Multiple Incidence Angle (MIA-HDS)' in previous project reports. These enhancements are summarized in Table 5-1. These terms should be treated as synonymous throughout the project documentation.

Table 5-1 Summary of Enhancements to Multi-Track HDS Solution

Enhancement	Description	Benefit
Improvement of the cross-stack registration and resampling	The method now refines the model used to spatially register two or more stacks acquired at different incidence angles by utilizing both the orbit derived stack image geometries and by cross-correlating the stack image data.	More robust and accurate spatial registration of image stacks which is important for subsequent joint processing steps.
Development of a joint stack based	The phase quality of each HDS target is now assessed using the phase information derived from all available data stacks.	Improved identification of coherent targets.

Enhancement	Description	Benefit
target quality measure		
Updating the configuration/logging interface	It is now simpler to configure the processing of multiple stacks of data and log the execution of different steps. The configuration is more logically organized and some of the configuration which repeats often is now centralized. This allows for cleaner directory/configuration structures and allows the user to easily browse and locate data and to easily configure and execute different processing steps.	Improved ease of use.
Updating the directory structure	The directory structure for MTI processing has been redesigned based on the issues identified when analyzing the results of the initial implementation. This as mentioned previously is to allow the user to be able to navigate the intermediate/final results more easily.	Improved ease of use.
Streamlining of initial steps	The initial processing steps of MTI have been streamlined by combining multiple small processing steps into a few larger coherent steps. This greatly simplifies the setup of the multiple data sets for MTI processing for the user.	Improved ease of use.
Sinc resampling	Existing bilinear interpolation of interferograms replaced by sinc function interpolator to reduce phase aliasing artifacts.	Less noise in final deformation estimates; more coherent targets retained.
Common footprint tool	Tool implemented to automatically compute polygon corresponding to footprint of all image stacks used. This simplifies selection of processing area of interest and determining which stacks to include during processing.	Improved ease of use.

5.3 Phase de-ramping for HDS Adaptive Filtering

The goal of this task was to implement and test a method for estimation and removal of local spatial phase gradients prior to HDS adaptive multi-looking. This has the potential benefit of reducing phase aliasing that can occur when ramped phase values are averaged.

The solution that was implemented is similar to that described in [R-12]. Rather than estimate an independent phase gradient for each interferogram, the algorithm solves for a set of model parameters corresponding to local 2D gradients of both residual topography and linear deformation rate by processing the entire network of interferograms jointly.

This method was implemented and tested using test data derived by imposing a simulated phase gradient pattern on a real interferometric stack. The results as shown in Figure 5-2 demonstrated that although the method was able to accurately estimate the parameter gradients for most targets, it failed on a subset of targets due the combined

effect of phase noise and small HDS neighbourhood size (estimates were derived over each adaptive neighbourhood). However in most real cases the fraction of targets with significant phase gradients is relatively small. Hence the implemented method reduces aliasing for the majority of this small target subset while introducing phase errors for a small fraction of all targets. The net effect in the simulated test case was an increase in phase errors rather than a reduction which was the goal of the method. For this reason, the implemented algorithm was not incorporated in the InSAR solution used for the project.

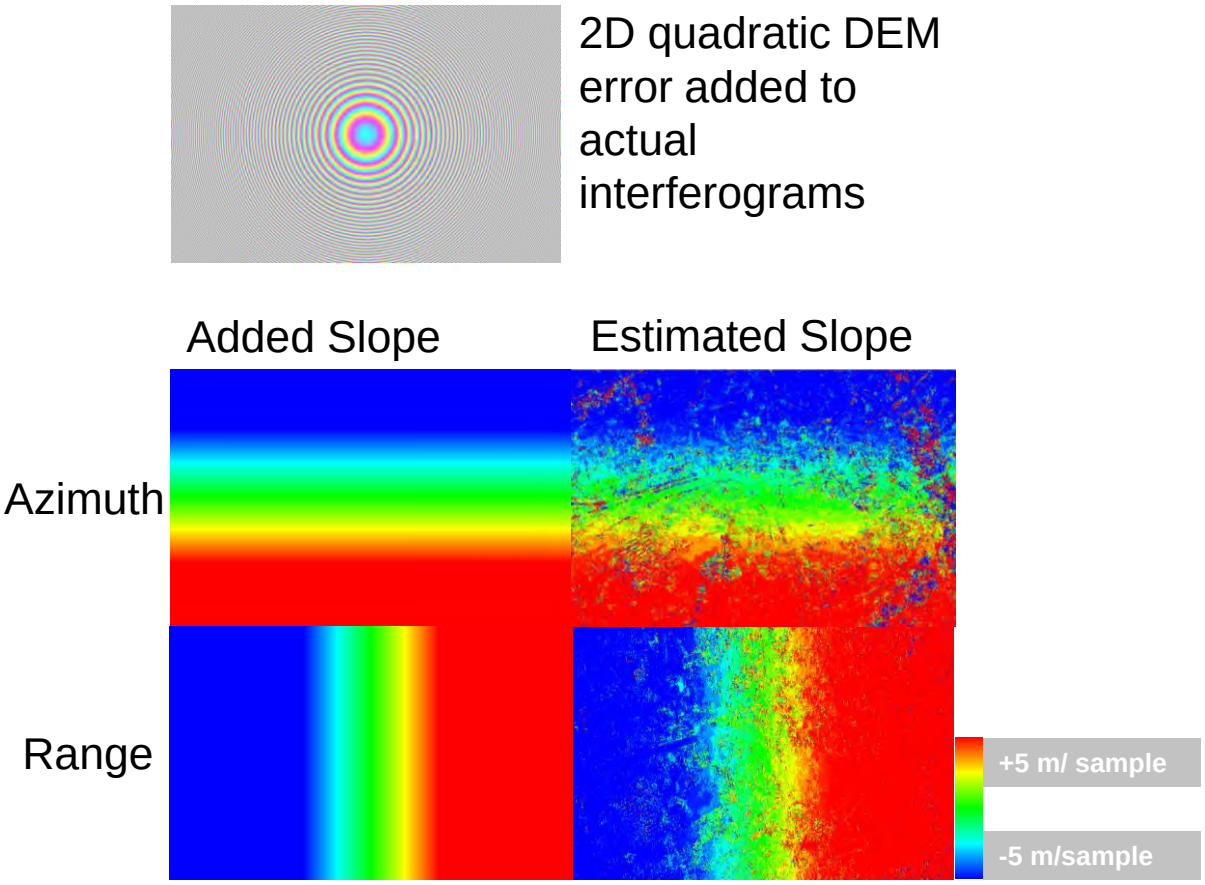

Figure 5-2 Simulation based test of phase de-ramping: (top) simulated quadratic topographic error 'bowl' superimposed on actual interferometric phase network; (bottom) azimuth and range components of true and estimated topographic slope.

5.4 Network phase unwrapping correction (L1—minimization)

The goal of this task was the implementation of a phase network inversion method that is robust to the presence of a small fraction of phase outlier values. One approach is to minimize the L1 residual phase norm rather than the L2 norm minimization that is achieved by using the existing method which uses the well-known Singular Value

Decomposition (SVD). This was conceived as a solution for mitigating the effects of increased phase unwrapping errors caused by using winter scenes during processing.

The goal of this task overlaps significantly with the goal of the Velocity based SVD network inversion (see Section 5.5) and also with that of the phase unwrapping error tool (see Section 5.8) and therefore this task was deemed unnecessary to allow inclusion of winter scenes during processing.

5.5 Velocity based SVD network inversion

This task addresses an issue that arises with the inclusion of winter scenes for InSAR processing. Winter scenes tend to only be coherent with other winter scenes acquired during the same winter. This is because the presence of snow alters the scattering distribution within a given resolution cell to such an extent as to destroy coherence with respect to the snow free state. Within winter coherence often occurs since changes in dry snow cover results in phase bias rather than significant changes to the spatial scattering distribution. Summer acquisitions however, may be coherent with other summer seasons both within a single summer and from year-to-year provided that the surface conditions do not result in significant temporal decorrelation.

These processes result in an InSAR phase network topology consisting of one connected sub-network corresponding to all snow-free scenes plus additional within-winter sub-networks that are not connected to any other sub-network. This poses a problem during phase network inversion since no coherent phase values exist to constrain the winter dates to the rest of the acquisition dates.

The developed solution uses the SVD to solve for the unknown deformation velocities within the observation period. Any velocities that are unconstrained by the phase network (e.g. those corresponding to summer-winter transitions) are estimated by the use of a locally weighted regression filter which is similar to assuming minimal acceleration over the unconstrained gap. Figure 5-3 and Figure 5-4 show comparisons between the existing and newly developed inversion methods for simulated and real data cases respectively.

The new method has been found to provide robust inversion for a variety of phase network topologies including those encountered by including winter-winter interferograms in the analysis of the project test sites.

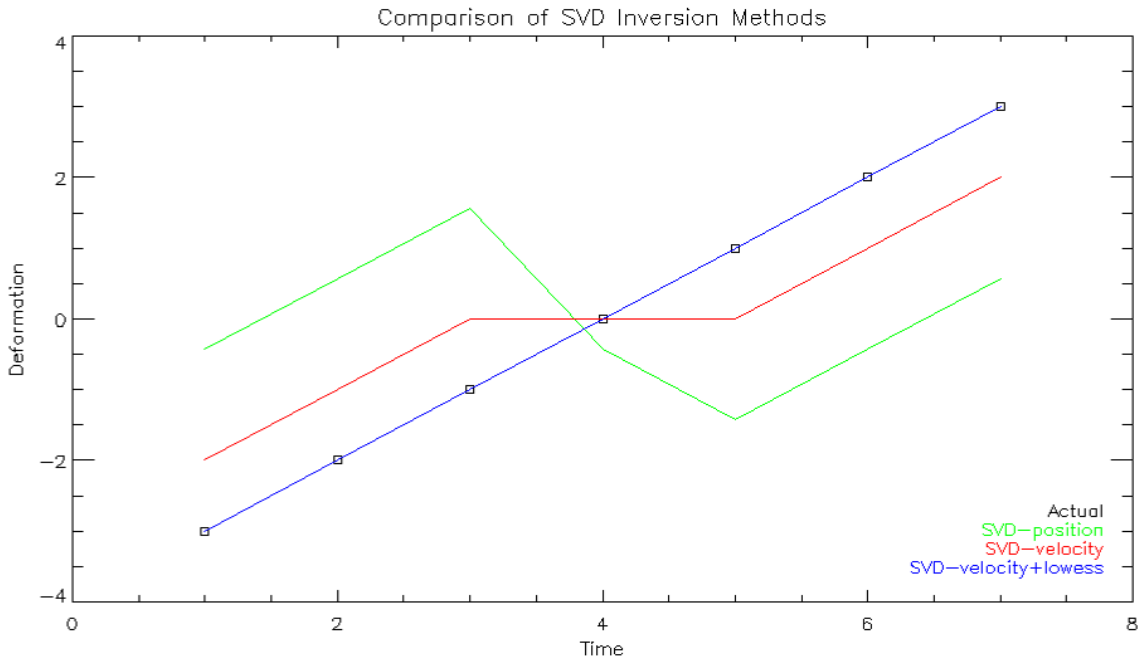

Figure 5-3 Simulation comparing various SVD based interferometric network inversion methods

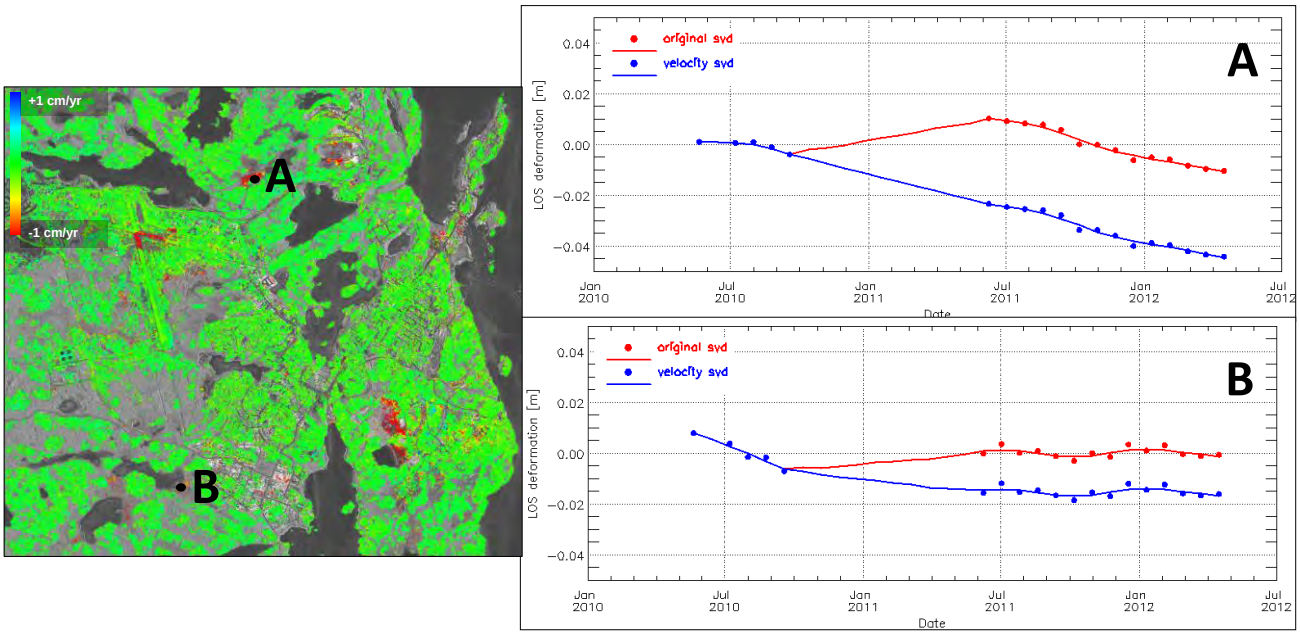

Figure 5-4 Deformation time series comparison of network inversion methods: (left) linear deformation rate map over Yellowknife. (right) sample deformation time series comparing the velocity and interpolation based SVD inversion with a position based SVD inversion.

5.6 Active layer model

Surface deformation in permafrost areas typically has a strong seasonal component due to the annual freeze/thaw cycle. Modelling and removal of this component was found to increase phase unwrapping performance and also to reduce seasonal bias effects in the estimation of long term deformation trends.

Phase unwrapping errors occur in areas containing high levels of phase noise or high spatial phase gradients. Interferograms spanning seasons (e.g. a spring-fall acquisition) may contain a significant phase component due to the difference in seasonal deformation present in the two acquisitions. Areas of the scenes corresponding to boundaries in near surface fractional ice volume will contain spatial phase gradients in these interferograms. The impact of these gradients on phase unwrapping performance can be mitigated by fitting a seasonal deformation model to the wrapped data prior to phase unwrapping. This is a similar approach as that used to fit and remove the residual topographic phase component prior to unwrapping.

The seasonal model used is similar to that described in [R-7] and derives a template for surface deformation with the surface temperature history as input. The modelled deformation is proportional to the square root of accumulated degree thaw days during the thaw period and the square root of accumulated degree freeze days during the freeze period.

This model assumes uniformity of the water content, pore fraction and thermal properties within the local ground column. It also assumes that the cyclic deformation either saturates during the freeze (corresponding to a true active layer reaching the permafrost during the freeze period) or during the thaw (corresponding to a frost layer not connected to the permafrost).

The surface temperature history for the sites was estimated by taking the daily mean air temperature as recorded by Environment Canada metrological stations in each community and adding a constant offset to account for the mean air-ground temperature difference. For Umiujaq, air temperature data and corresponding data from the three thermistor monitored bore holes were used to estimate a year-round average air-to-ground temperature difference of 4.3 degrees C. This same value was used for Salluit. For the Beaver Creek and Yellowknife sites a value of 5.0 degrees C was assumed.

Figure 5-5 shows the mean daily air temperature history and corresponding seasonal deformation template for Umiujaq from July 2012 to November 2014. This template shows an uplift phase from November – May and a subsidence phase from May – September. Figure 5-6 compares the frequency of phase unwrapping errors with and without the use of a seasonal deformation model to remove seasonal phase components prior to unwrapping and shows a clear reduction in error frequency with the use of the model.

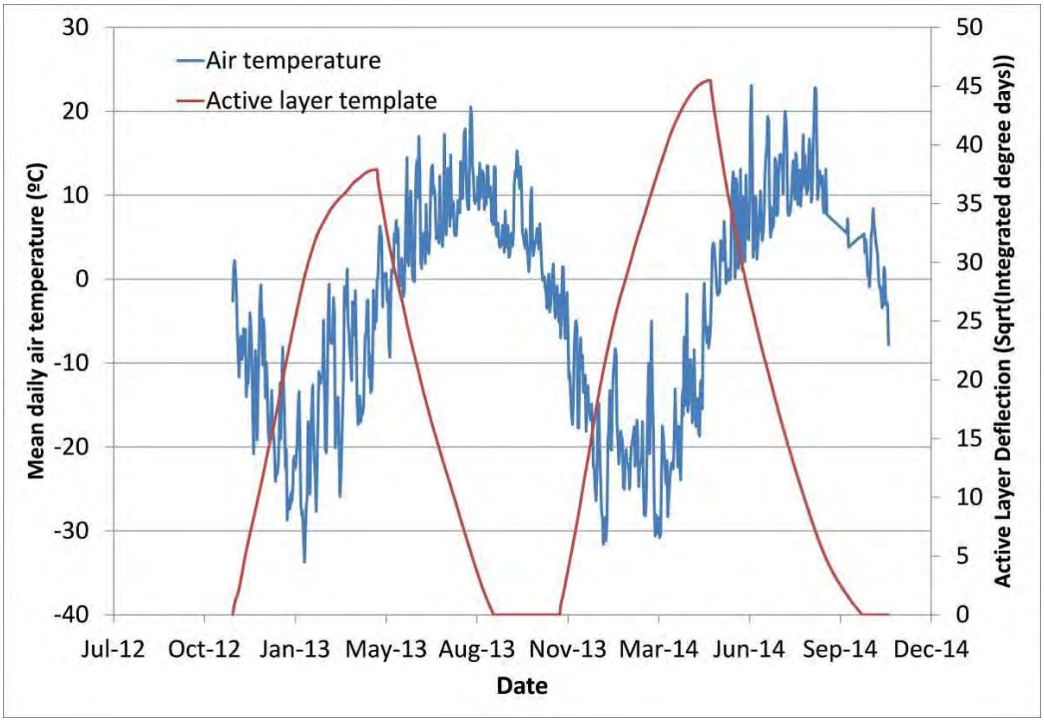

Figure 5-5 Mean daily air temperature and corresponding active layer template for Umiujaq test site.

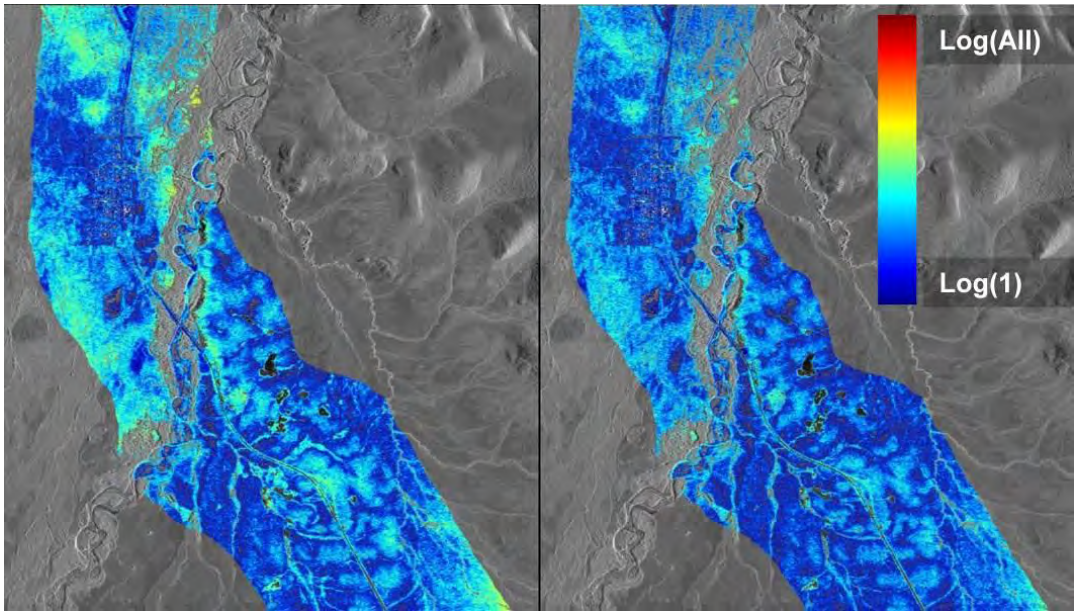

Figure 5-6 Phase unwrapping error density maps for the Beaver Creek RADARSAT-2 stacks : (left) using no demodulation and (right) demodulation incorporating active layer template.

5.7 Masked processing

InSAR monitoring of highways involves estimating deformation around some corridor that follows the highway route. The area of interest is therefore often long, narrow and curved. This results in a significant inefficiency in the use of computer resources (both processor time and disk storage) when images are processed as rectangular subsets. This task involved a restructuring of data storage format, methods for iterating over spatial samples and data rendering methods to allow for the definition and processing of arbitrary non-rectangular AOIs. For both Umiujaq and Beaver Creek test sites this resulted in a 50% reduction in processing time and disk usage over what could be achieved with rectangular subsets. Figure 5-7 show sample masked defined AOIs defined for both Umiujaq and Beaver Creek sites. It is expected that for wide scale highway monitoring applications the improvement factor could be much larger than for those shown here. For example, a highway running diagonally through a 2500 km^2 wide Ultrafine scene monitored with a 100 m corridor (50m on either side) would enjoy a 99.7% reduction in processed area.

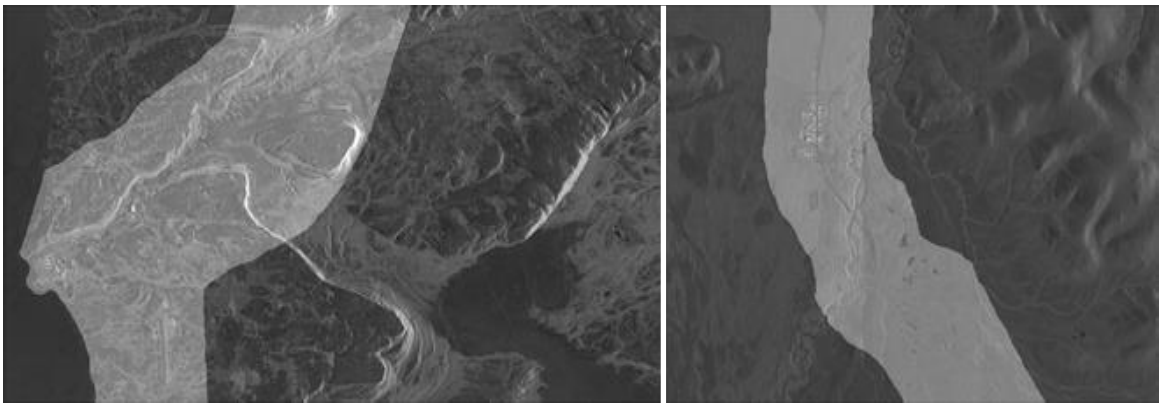

Figure 5-7 Regions of interest used for Umiujaq (left) and Beaver Creek (right)

5.8 Phase unwrapping error tool

The inclusion of winter scenes has the potential to result in an increased number of phase unwrapping errors during processing. A tool was therefore developed to estimate and display the distribution of phase unwrapping errors that occur during processing. This allows for interactive inspection and adjustment of parameters including the selection of which interferograms to include in processing.

The concept behind the tool is that for a given spatial sample, in the absence of unwrapping errors the network of interferometric phase values will form a nearly linearly consistent set with deviations only due to a spatial decorrelation related noise term. This network is numerically inverted to derive per acquisition phase values and then reconstructed to produce a perfectly linearly consistent phase network. The difference between the original and reconstructed phase networks represents an estimate of the phase error in each interferogram. Phase errors near or exceeding 2*pi are

assumed to be due to an unwrapping error in that interferogram. A suitable threshold less than 2*pi is therefore selected and all samples with estimated phase errors exceeding this value are flagged as likely phase unwrapping errors.

The distribution of these detected errors can be rendered both as a spatial map (number of errors occurring at each spatial location) and as a network matrix plot (number of errors occurring in each interferogram). Figure 5-8 and Figure 5-9 show examples of these renderings for the Umiujaq site both before and after the exclusion of problematic summer-winter interferograms. These show a significant reduction in unwrapping errors with the removal of the summer-winter interferograms.

This tool proved invaluable during the processing of all project sites as a means for identifying and removing problematic interferograms.

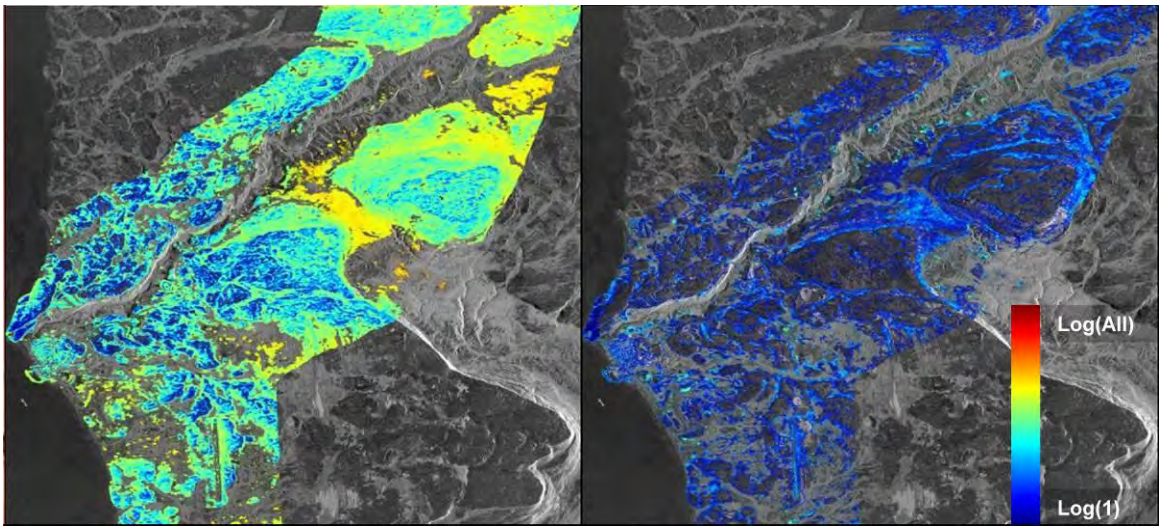

Figure 5-8 Phase unwrapping error density maps for the Umiujaq RADARSAT-2 stacks: (left) using full interferometric network and (right) winter-summer pairs excluded.

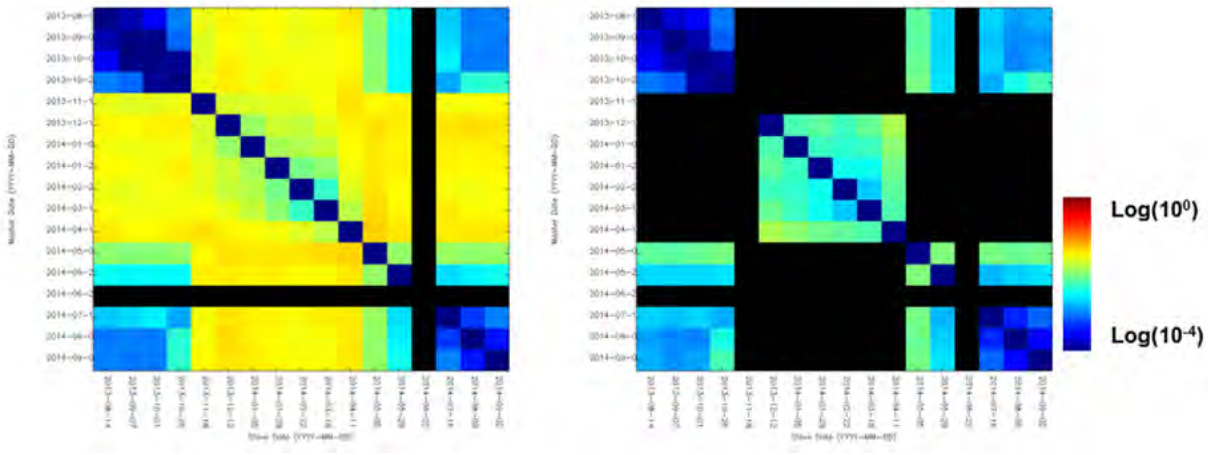

Figure 5-9 Phase unwrapping error density network matrices for Umiujaq RADARSAT-2 stacks: (left) using full interferometric network and (right) winter-summer pairs excluded.

5.9 Transect tool

Some work was done to develop a tool to extract and display InSAR results along user defined curvilinear transects. This is beneficial for reporting InSAR monitoring results over highways which are often specified and managed according to a distance marker system. Commercial GIS tools typically allow for the extraction of transect data from 2D datasets. However there is some benefit to having a transect functionality implemented as part of the InSAR solution software since this allows for extraction and reporting of any spatial information generated during InSAR processing within the context of the defined transect. Figure 5-10 shows an example of using the implemented transect tool to extract coherence information along a highway road surface. This provides the InSAR analyst information about which interferograms contain coherent information regarding the road surface itself.

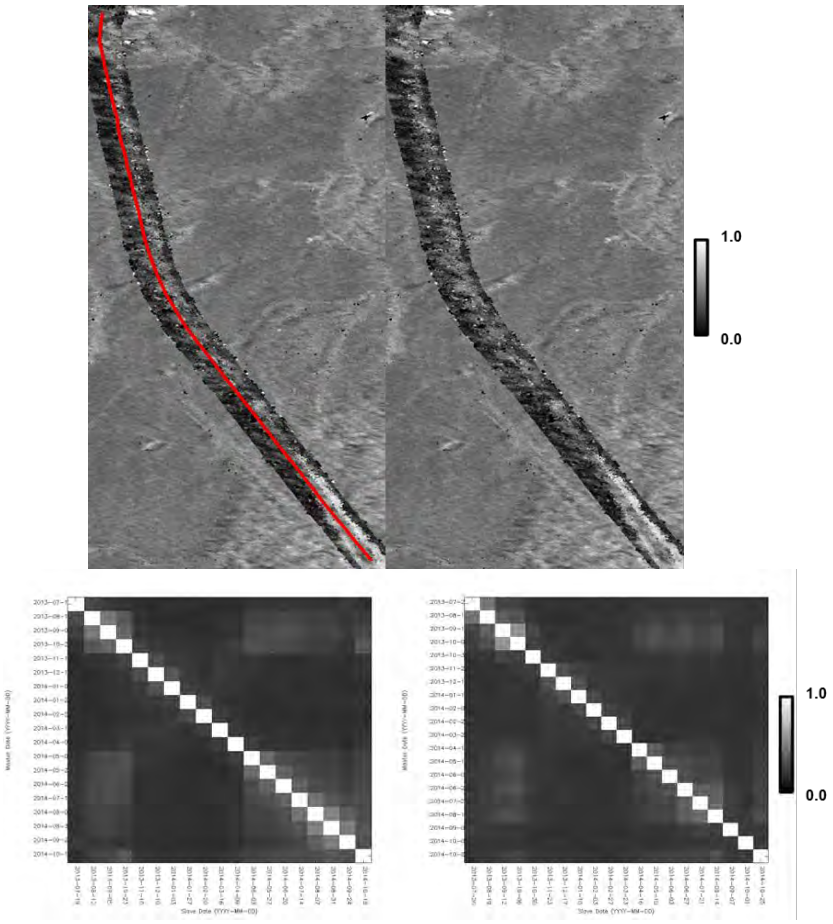

Figure 5-10 Transect tool example showing extraction and display of coherence estimates along highway road surface near Beaver Creek : (top) road following transect overlaid on single coherence image; (bottom) network coherency matrices for all samples along transect showing seasonal coherence behavior for road surface.

6 INSAR ANALYSIS

6.1 Yellowknife

The two RADARSAT-2 Ultra-fine descending stacks were the first InSAR stacks processed during the project and were used to develop the methods described in Section 5. InSAR image stacks used for this site are summarized in Figure 6-1, showing the image footprints and processed area and Table 6-1, which contains a summary of image parameters. A surficial geology map of the region [R-8] shows the processed area to be primarily bedrock, glaciofluvial and glaciolavustrine sediments with small areas of organic deposits. Downtown Yellowknife and the airport are built primarily over glaciofluvial sediment areas whereas the developed area to the south-west of downtown is built primarily on glaciolacustrine/bedrock areas. The processed subset area was selected to cover the city and airport and to coincide with areas covered by the available surficial geology map and DInSAR results derived from summer 2010 U19 stacks images published by Stephen Wolfe et al. [R-9].

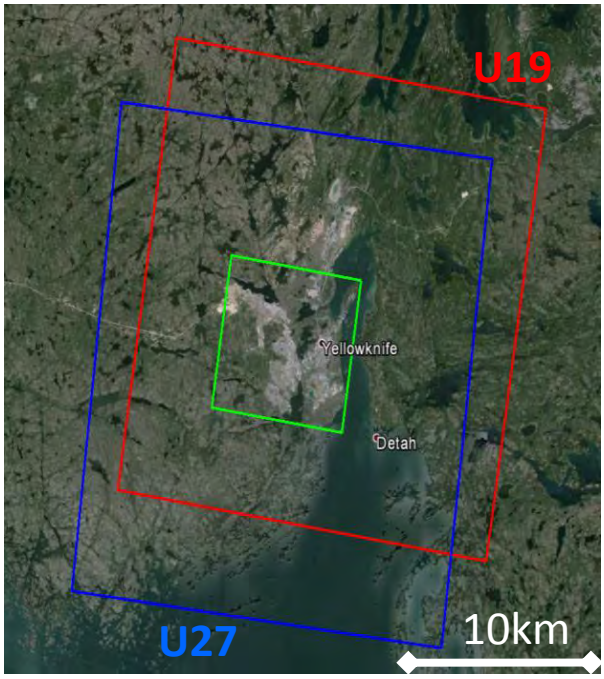

Figure 6-1 Yellowknife RADARSAT-2 Ultra-fine stack footprints showing processed subset (green rectangle).

Table 6-1 RADARSAT-2 data processed for Yellowknife

	Beam Mode	
	U19	**U27**
Number of scenes processed	26	33
Incidence angle	44º	49º
Processed data start date	May-2010	Oct-2009
Processed data end date	Jun-2013	Jun-2013

Figure 6-2 shows the surficial geology map along with the Multi-Track HDS InSAR model component estimates and the DInSAR displacement map. The HDS InSAR results show a few areas of limited magnitude linear deformations. Most notably these include:

- subsiding area on the airport runway know to correspond to an unstable area of near surface clays [R-10].
- uplift occurring along a section of Old Airport Road
- subsidence in dump/industrial area immediately north of Jackfish lake

The HDS InSAR results show extensive areas of significant seasonal deformation which correlate well with the absence of bedrock. The published DInSAR results show a spatial correlation with the HDS seasonal results. Since the DInSAR results are generated over a single summer, they do not discriminate between linear and seasonal deformation which is primarily downward over the snow free period.

This comparison shows the benefit of modeling both seasonal and linear deformation based on year-round measurements rather that stacking summer only interferograms since the deformation is dominated by the seasonal component which can mask the true long term deformation component.

The HDS results show more incoherent areas than for the DInSAR result which is likely due to the fact that the DInSAR result was estimated from images from a single summer hence yielding on average higher coherence interferograms.

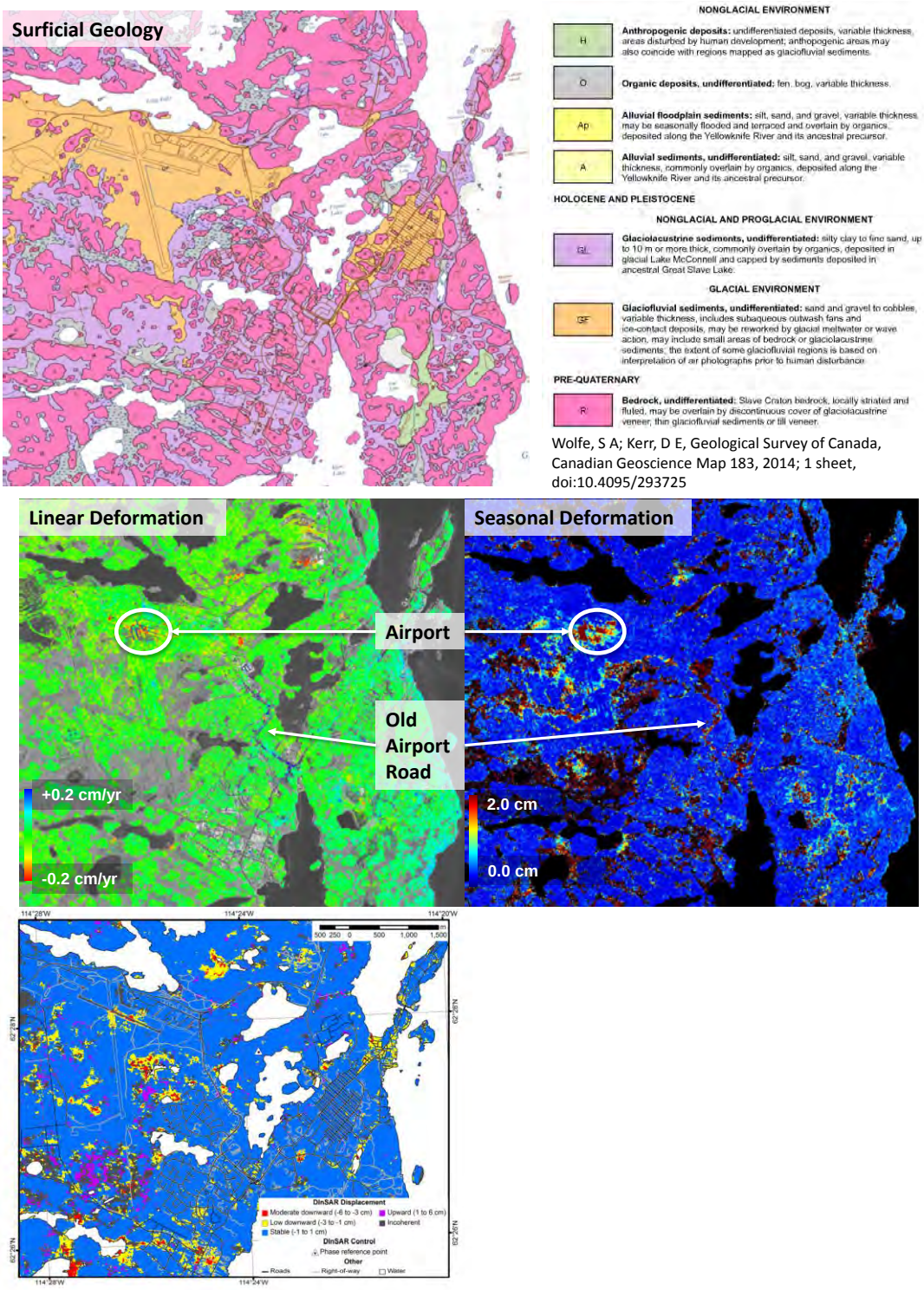

Figure 6-2 Comparison of results for Yellowknife test site : (top) Surficial geology, (centre) to Multi-Track HDS InSAR deformation model component estimates projected to vertical and (bottom) summer 2010 only displacement estimates estimated by Wolfe, S et al. [R-9].

6.2 Salluit

Salluit Multi-Track HDS InSAR deformation estimates were generated by processing two TerraSAR-X ascending spotlight stacks. InSAR image stacks used for this site are summarized in Figure 6-3, showing the image footprints and processed area and Table 6-2, which contains a summary of image parameters. The processing subset area was selected to include the village and airport road. Most of the runway was not included because it falls outside of the ST17 stack footprint. The stacks cover a 22 month time period and include two snow free seasons.

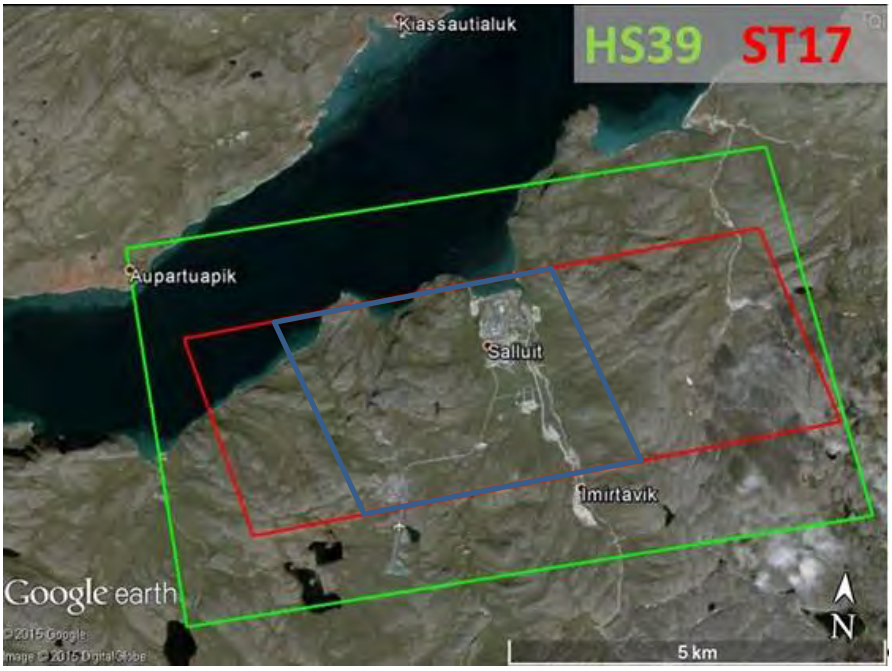

Figure 6-3 Overlay of Salluit TerraSAR-X ascending footprints over Google Earth. Processed subset is shown in blue.

Table 6-2 TerraSAR-X data processed for Salluit

	Beam Mode	
	HS39	**ST17**
Number of scenes processed	44	44
Incidence angle	34.7º	24.6º
Processed data start date	2013-12-27	2014-01-02
Processed data end date	2015-10-29	2015-10-24

A surficial geology map of the Salluit area was provided by CEN. This is shown along with the HDS InSAR linear and seasonal deformation model component maps in Figure 6-4. The spatial coverage of coherent targets is generally very good. However the

coherent target coverage on the roads is sparse which is likely due to disturbance of the unpaved surface. Areas corresponding to bedrock generally show no or limited linear and seasonal deformation. Notable areas with linear deformation include:

- small subsiding area on slope immediately west of the main village near storage tanks.
- small subsiding area on east facing slope south of the main village site, near water storage tank.
- subsiding areas on slope west of airport road to the southwest of village
- uplift observed in village areas (main village area and also area of recent construction to the south)

There are several areas with significant seasonal deformation including some within the main village and in areas corresponding to thick till deposits and deep marine sediments.

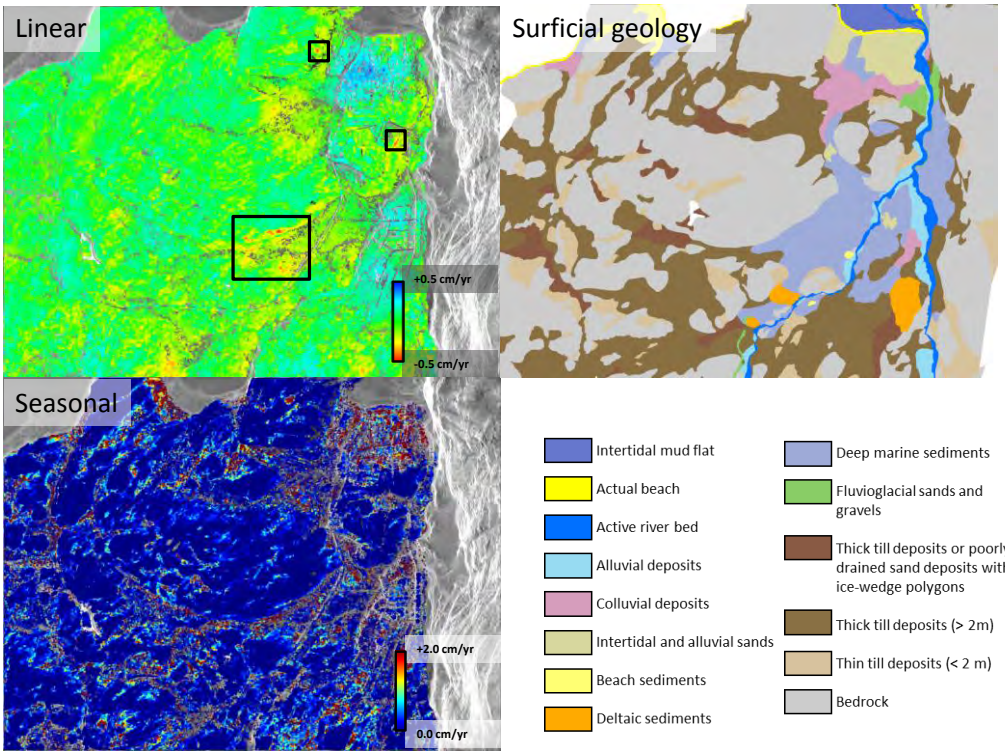

Figure 6-4 Comparison of surficial geology to deformation model component estimates from two Salluit TerraSAR-X stacks. Examples of subsiding areas near infrastructure are highlighted in top-left linear deformation panel.

An example time series for the subsiding slope near the water tank is shown in Figure 6-5. This target exhibits a nearly linear subsidence of ~1 cm over the 21 month monitoring period with a low amplitude seasonal component (~0.5 cm peak-to-peak). The inset linear deformation map shows spatial patterns that correlate with locations of buildings and roads as shown in Google Earth.

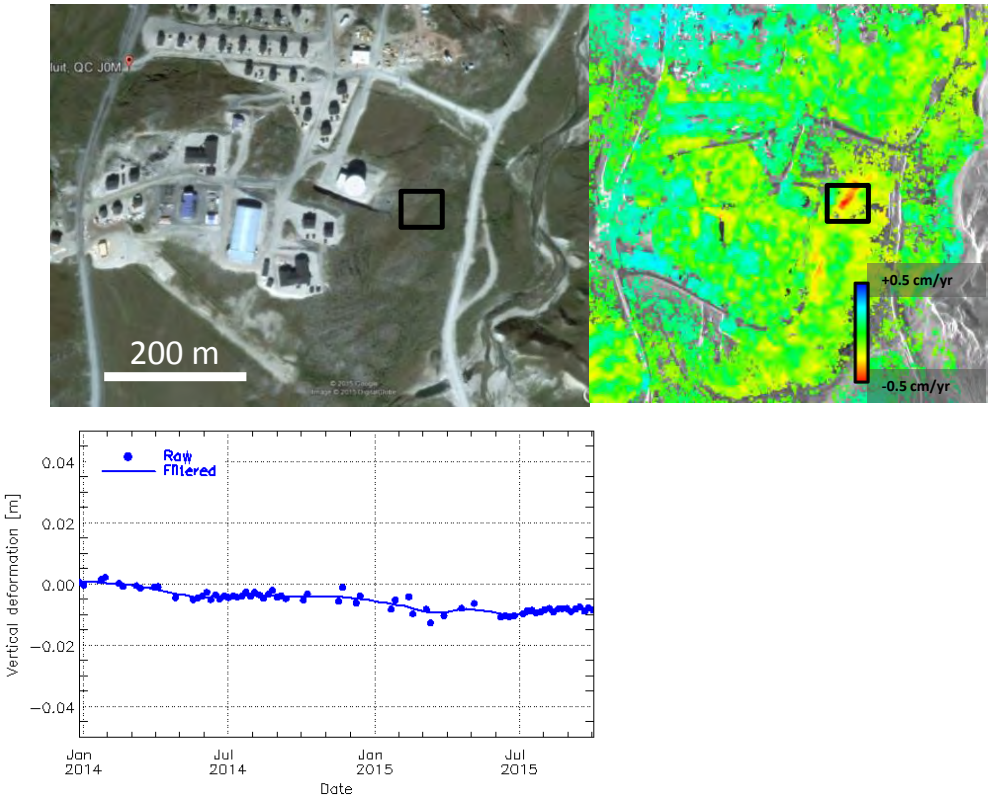

Figure 6-5 Example deformation time series for point of deforming slope adjacent to water storage tank.

6.3 Umiujaq

6.3.1 InSAR Products

The primary InSAR deformation results for Umiujaq were generated using three RADARSAT-2 Spotlight mode stacks. InSAR image stacks used for this site are summarized in Figure 6-6, showing the image footprints and processed area and Table 6-3, which contains a summary of image parameters. The processing subset area was selected to include the village, airport road, airport as well as the alluvial valley running north-east from the village and the Tasiapik valley. The stacks cover a 33-month time period and include three snow free seasons.

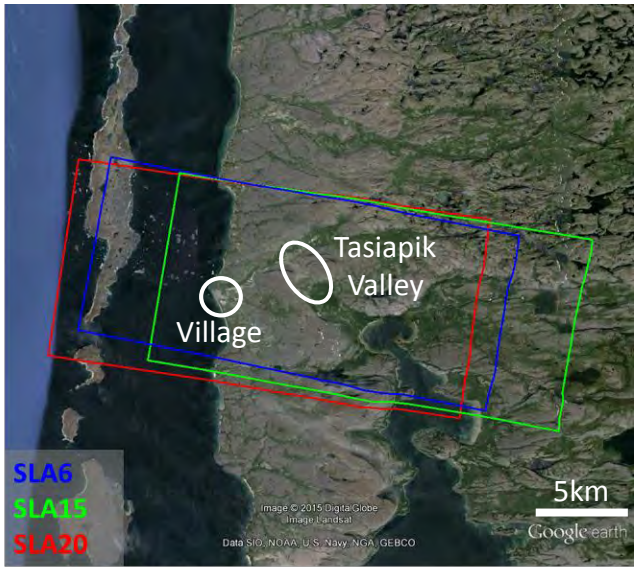

Figure 6-6 RADARSAT-2 data stacks processed over Umiujaq

Table 6-3 RADARSAT-2 data processed over Umiujaq

	Beam Mode		
	SLA6	**SLA15**	**SLA20**
Number of scenes processed	33	38	34
Incidence angle	34.7º	41.4º	44.8º
Processed data start date	2013-08-14	2013-01-24	2013-07-18
Processed data end date	2015-10-15	2015-10-29	2015-10-12

Figure 6-7 and Figure 6-8 show the linear and seasonal LOS deformation components. Note that the multiplicative factor to convert the magnitude of these values from LOS to vertical deformation is 1.33. Insets for specific areas of interest are shown highlighted. The coherent target spatial coverage is very high in all areas except some of the alluvial valley and the area to southwest of the Tasiapik valley. Many areas show little or no subsidence and this can be attributed to the fact that surficial rock is the most common surficial geology type in the processed area. However, many localized areas of linear and seasonal deformation are present in the scene and these can be shown to correspond to non-rock areas.

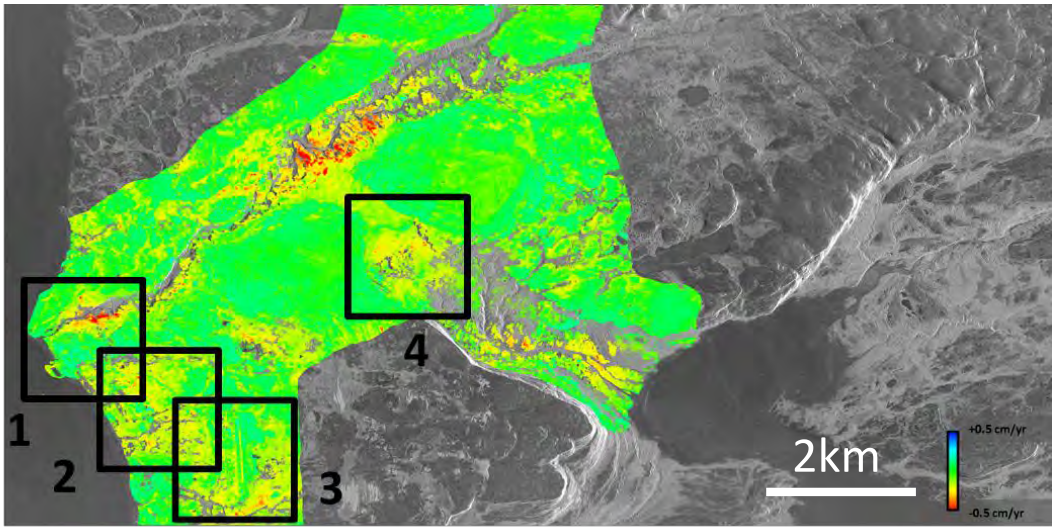

Figure 6-7 LOS linear deformation rate estimate over Umiujaq with insets shown for (1) town site, (2) airport road, (3) airport and (4) Tasiapik Valley.

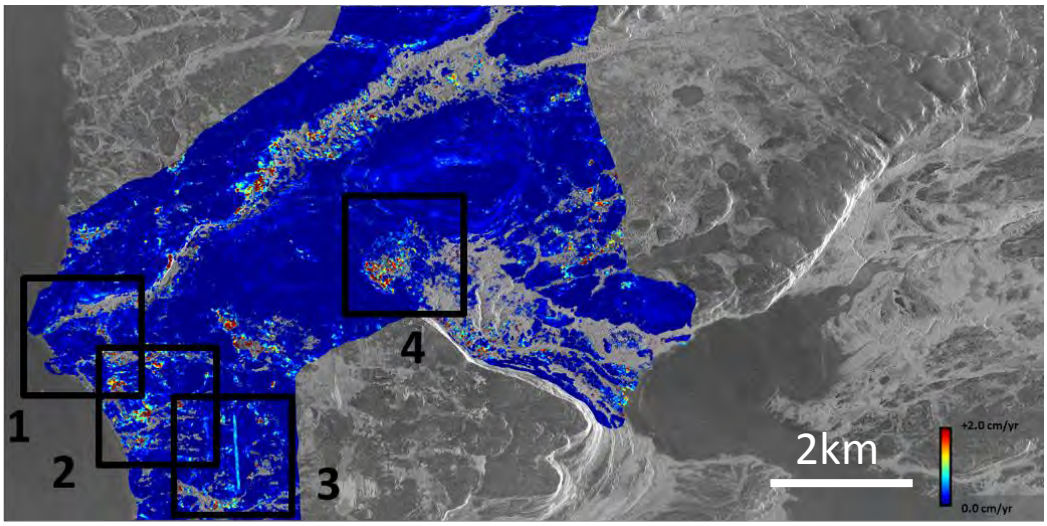

Figure 6-8 LOS seasonal motion amplitude estimate over Umiujaq with insets shown for (1) town site, (2) airport road, (3) airport and (4) Tasiapik Valley.

Linear and seasonal deformation maps for the subsets are shown below in Figure 6-9 to Figure 6-12. The village inset shows wide area subsidence of the river facing slope north of the village. There is a small area of subsidence within the main village which has not been attributed to any specific cause. There is also observed subsidence in the newly developed area immediately south of the main village which is likely due to consolidation of the recently constructed gravel pads. The airport road is coherent and

although generally stable, includes a short section of subsidence with magnitude < 0.5 cm/yr LOS.

There is an area known to contain lithalsas as reported in [R-11] and shown in Figure 6-9. This area shows somewhat sparse coherence and spatially variable estimates of the seasonal component which are suspected to contain errors due to phase unwrapping problems induced by high spatial phase gradients associated with the deforming lithalsa

It is noteworthy that most of the road surfaces show a net positive difference in linear deformation rate compared to their immediate surroundings. For example, in the village roads show a very weak uplift relative to the surrounding surfaces. The airport road (with the exception of the noted subsidence zone) appears stable compared to most surround areas which show a slight subsidence.

The airport shows subsidence to either side of the runway but not on the runway itself. However the entire runway surface has a notable higher seasonal deformation magnitude which may be due to the runway being kept snow free over the winter.

The final inset shows the Tasiapik Valley which shows subsidence in most areas of the valley itself and small patches of higher magnitude subsidence.

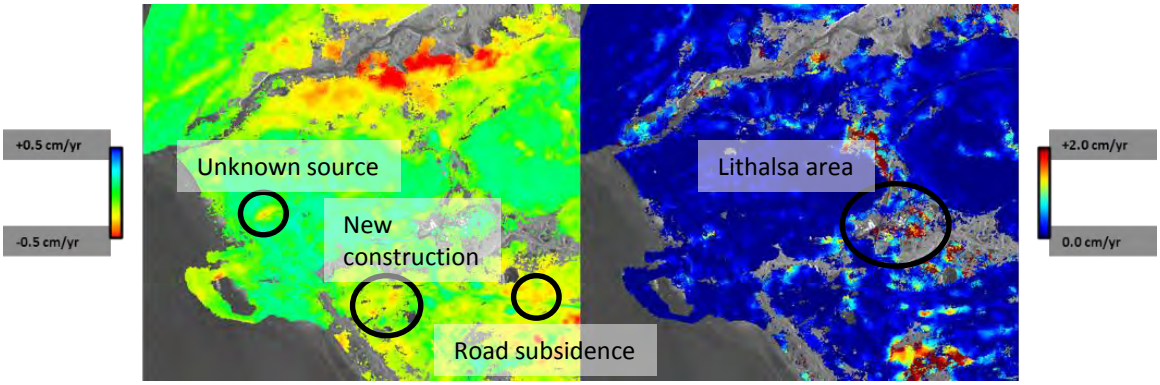

Figure 6-9 LOS linear deformation (left) and seasonal motion (right) over the Umiujaq village.

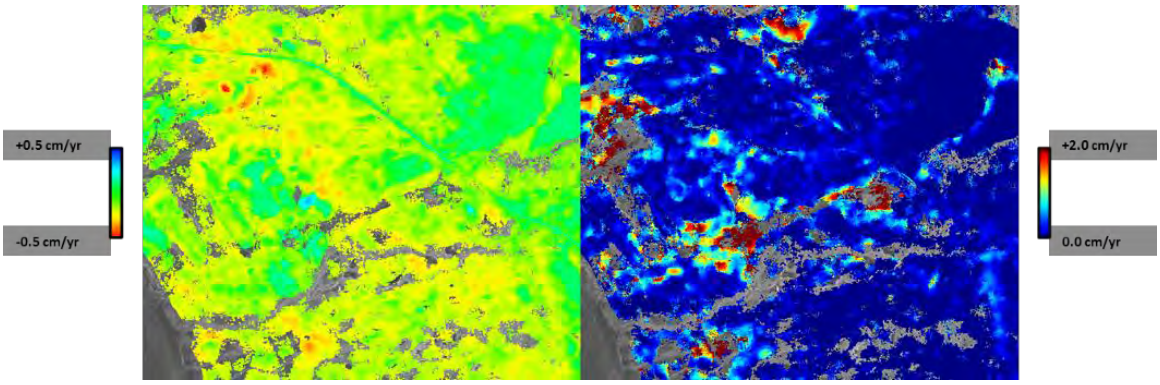

Figure 6-10 LOS linear deformation and seasonal motion maps over road between Umiujaq village and airport.

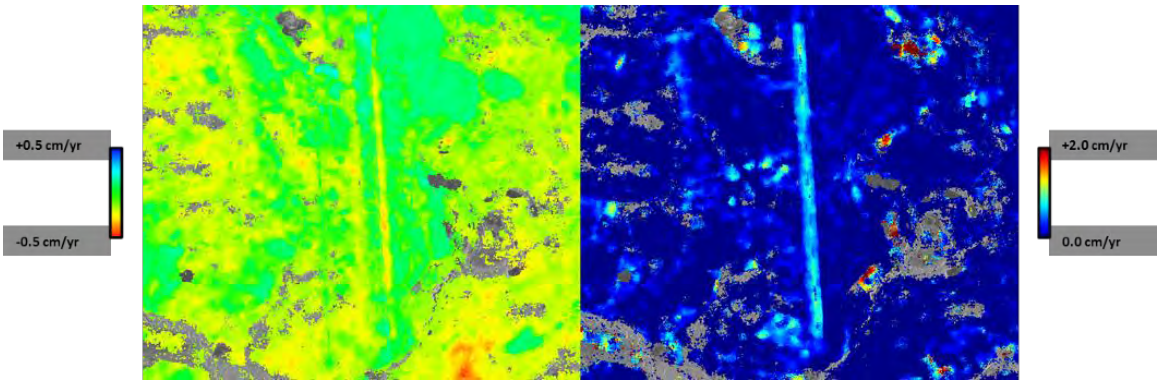

Figure 6-11 LOS linear deformation (left) and seasonal motion (right) over airport.

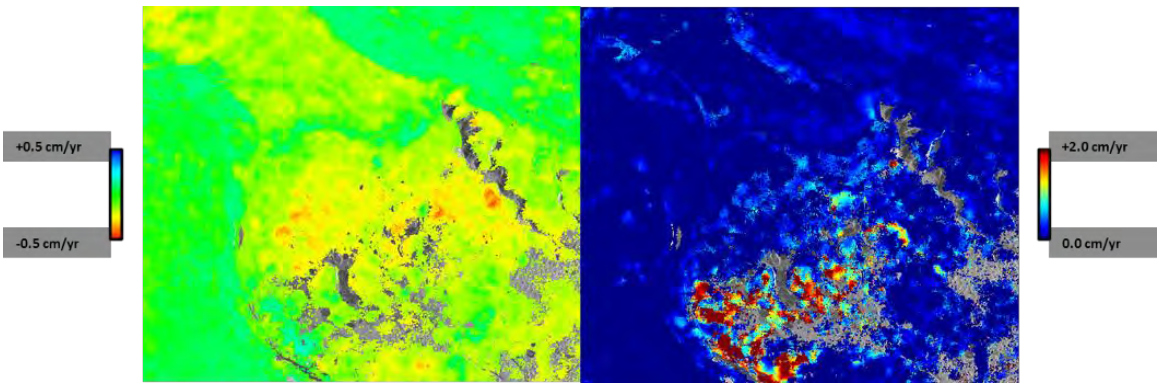

Figure 6-12 LOS linear deformation (left) and seasonal motion (right) over portion of Tasiapik Valley.

6.3.2 Corner Reflectors

A total of five floating and two anchored corner reflectors (CRs) were installed and maintained by CEN at the Umiujaq site as shown in Figure 6-13. Figure 6-14 to Figure 6-21 show the deformation time series for all CRs for the reflector itself and for the surrounding area (annulus of 13x13 multi-looked spatial samples).

Figure 6-13 Location map of the floating and anchored CRs

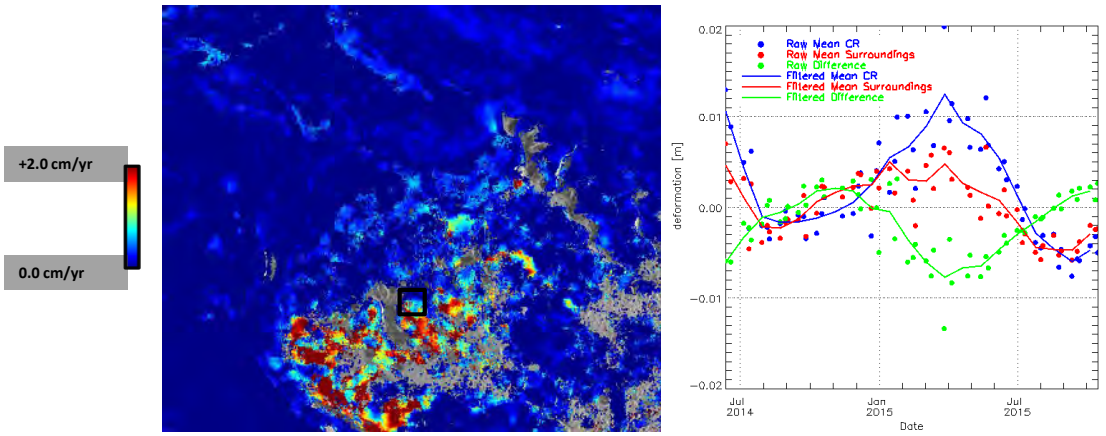

Figure 6-14 LOS deformation trace for anchored CR A1 starting June 2014.

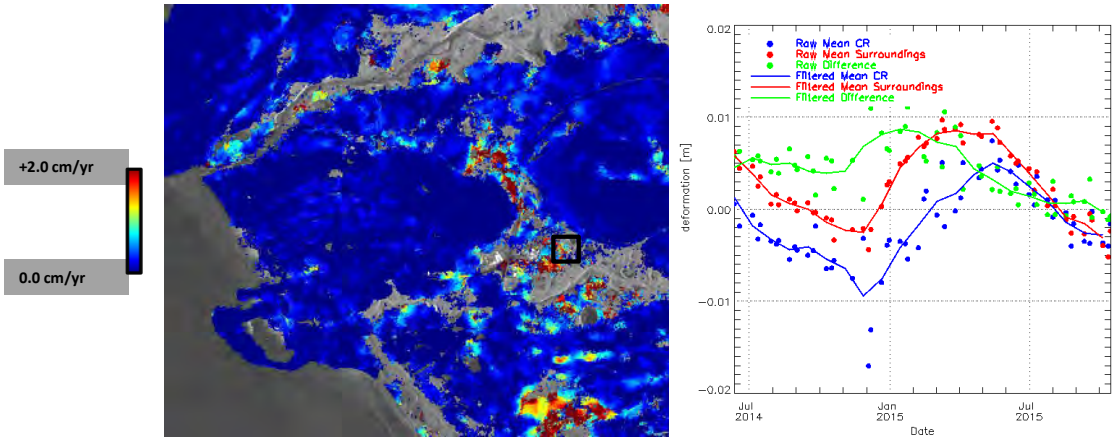

Figure 6-15 LOS deformation trace for anchored CR A3 starting June 2014.

For the two anchored CRs the deformation values were interpolated at the dates corresponding to CEN scratch test measurements. The InSAR CR deformation

estimates were subtracted from the surrounding annulus estimates to derive a value that one might expect to correlate with the scratch test data. These results are summarized in

Table 6-4 and show that the InSAR results do not correlate with the scratch test results. CEN has reported that the anchored reflectors were installed on palsas so the area in the immediate vicinity is expected to exhibit significant deformation. An analysis of the anchored CR temporal coherence magnitude shows that they both exhibit significantly lower coherence than most other spatial samples in the Umiujaq processed area (shown in Figure 6-16). This is likely due to the fact that the anchored CRs experience significantly less deformation relative to their respective local reference areas of the rapidly deforming lithalsa. The phase values for these CRs are therefore corrupted by phase unwrapping errors which results in the observed discrepancy with respect to the scratch gauge measurements. In future studies, to avoid similar problems anchored reference CRs should not be installed on lithalsas or similarly active features.

Table 6-4 Comparison of anchored CR scratch gauge measurements to InSAR cumulative differential deformation estimates (differences between CR and local annulus mean).

		Date		
		06/2014	**10/2014**	**09/2015**
A1	**InSAR - surface(cm)**	0.7	0.0	-0.7
	InSAR - CR (cm)	1.3	-0.1	-0.8
	InSAR - difference (cm)	-0.7	0.1	0.1
	InSAR cumulative difference (cm)	0.0	**0.8**	**0.8**
	Scratch gauge (cm)	0	**-9**	**-13**
A3	**InSAR - surface(cm)**	0.8	-0.1	-0.1
	InSAR - CR (cm)	0.1	-0.7	-0.3
	InSAR - difference (cm)	0.7	0.5	0.1
	InSAR cumulative difference (cm)	0.0	**-0.1**	**-0.5**
	Scratch gauge (cm)	0	**-5**	**-7**

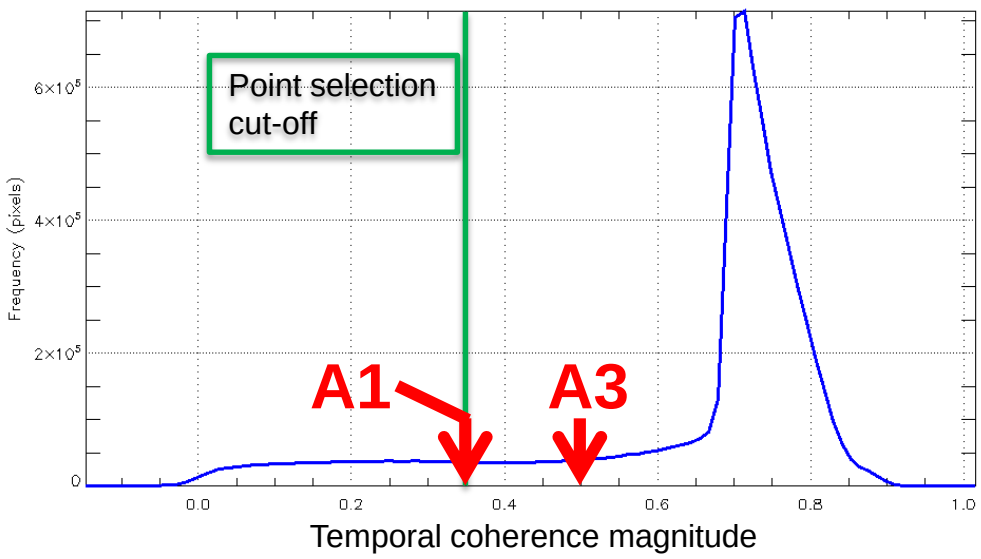

Figure 6-16 Comparison of anchored CR temporal coherence with distribution from all spatial samples in Umiujaq processed area.

Traces for the floating CRs are shown below. Note that CR F1 and CR F2 experienced snow infiltration and experience more phase noise up to the summer of 2014.

CR F1 shows good agreement with the surrounding annulus mean.

CR F2 shows good agreement only after the correction of the snow infiltration issue.

CR F3 appears to show low phase noise but very large seasonal variation while the surrounding annulus estimates show almost no seasonal variation.

CR F4 shows a higher (~2x) seasonal variation than the surrounding annulus area.

CR F5 shows good agreement with the surrounding annulus area.

It is noteworthy that all floating CRs appear to exhibit a net subsidence over the monitoring period.

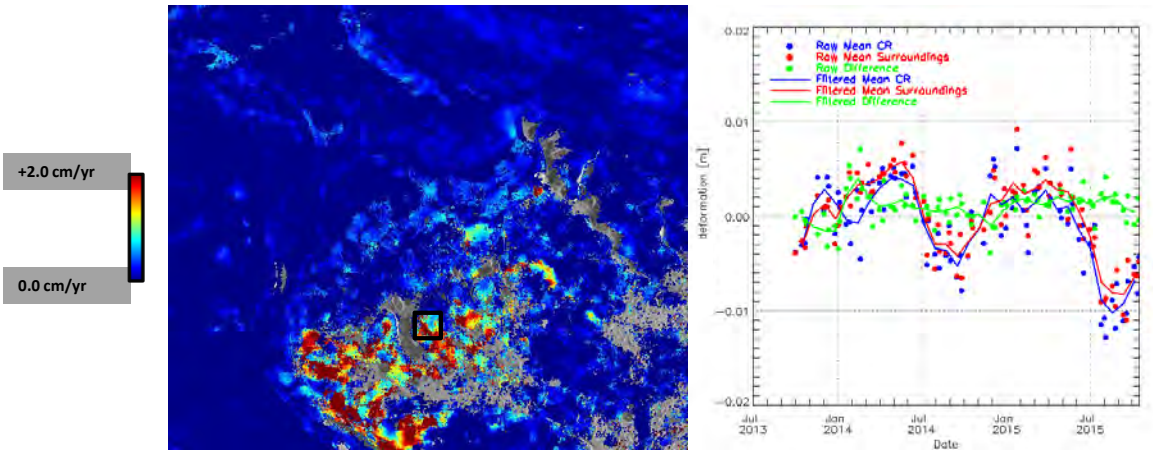

Figure 6-17 LOS deformation trace for floating CR F1 starting October 2013.

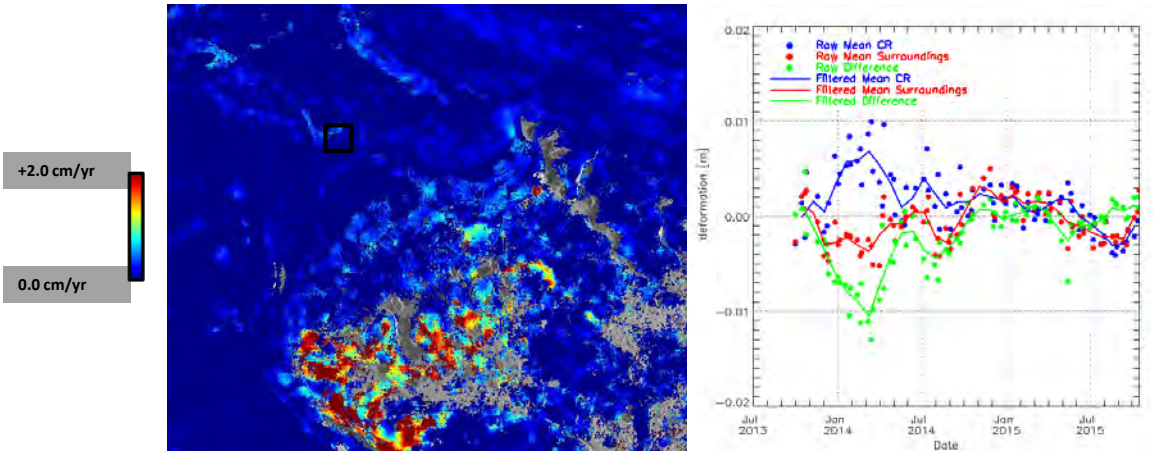

Figure 6-18 LOS deformation trace for floating CR F2 starting October 2013.

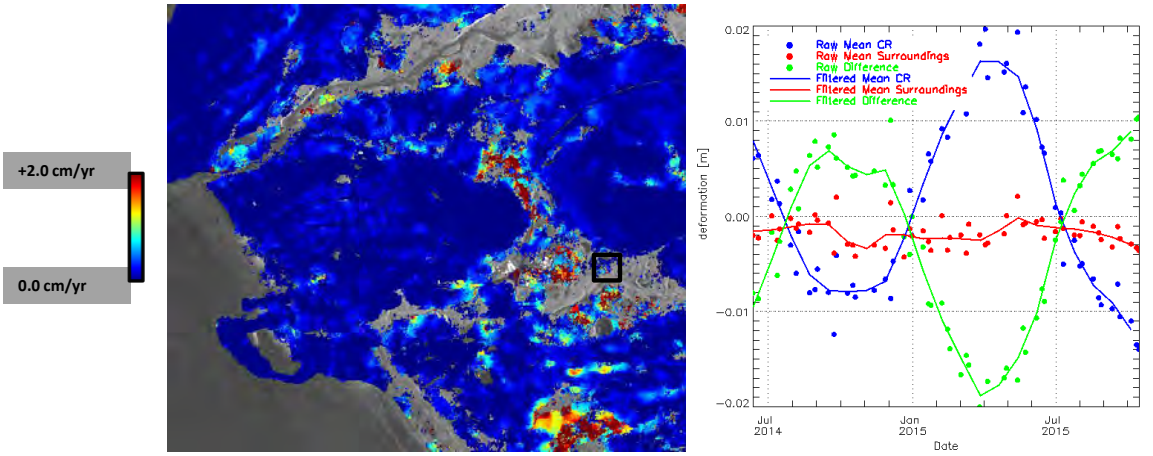

Figure 6-19 LOS deformation trace for floating CR F3 starting June 2014.

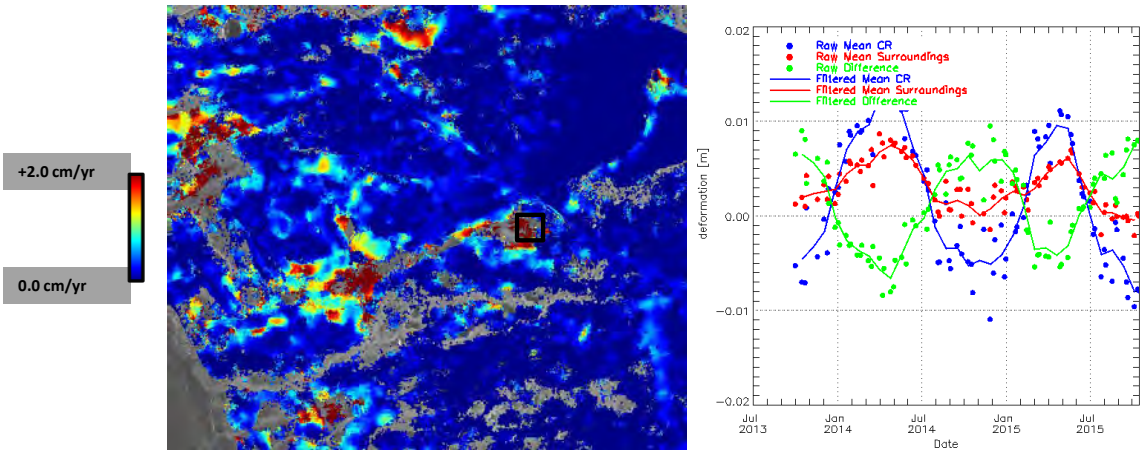

Figure 6-20 LOS deformation trace for floating CR F4 starting October 2013.

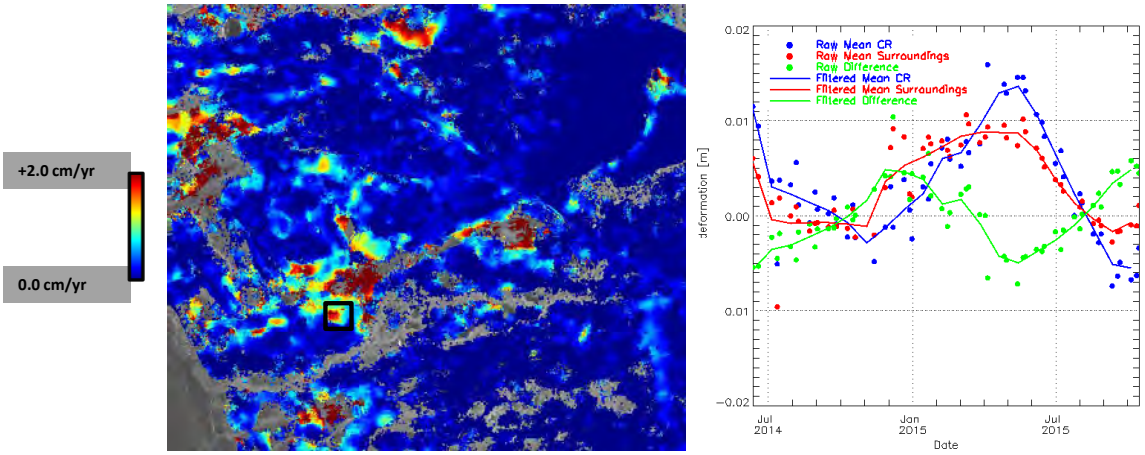

Figure 6-21 LOS deformation trace for floating CR F5 starting June 2014.

6.3.3 Surficial Geology Analysis

Some work was done to look at the distribution of deformation magnitudes by surficial geology type. The surficial geology map for Umiujaq provided by CEN shows significant variation in surficial geology within the area of interest defined by the village, airport, connecting road and also the Tasiapik valley. It is clear from a casual comparison of this map and the Umiujaq deformation estimates that a correlation exists between the deformation estimates and the surficial geology classification. We examined the degree of variation in deformation magnitudes within the surficial geology classes to determine whether the InSAR deformation maps add new information over what is already provided by the surficial geology maps. Figure 6-22, Figure 6-23 and Figure 6-24 show these distributions for the temporal coherence magnitude, linear deformation component and seasonal deformation components respectively.

For the bedrock class these show narrow distributions for all three parameters. The coherence magnitude is centered at ~0.7 which corresponds to relatively high coherence

considering that winter scenes were included in this assessment. Both the linear and seasonal components are centered near zero which is as expected since these are not expected to exhibit deformation. These bedrock results provide some validation of the deformation results and an indication of the measurement uncertainties for targets with similar coherence magnitudes (i.e. near 0.7). Both littoral sediments and eolian (windblown) deposits show similar distributions for all three parameters. They exhibit relatively high median coherence magnitudes (~0.7) but with a higher variance than that of bedrock. They show primarily negative linear deformation (i.e. subsidence) with median values ~ -1.5 mm/year and seasonal components centered at zero. Glaciofluvial and alluvial deposits show similar behavior with wide coherence distributions centered at ~0.5. They show similar linear deformation distributions as for the littoral sediments and eolian deposits. The seasonal component distributions are generally positive and show peak-to-peak seasonal displacements up to ~2 cm. The other three classes (colluvial deposits, till deposits and beach deposits) represent very small fractions of the study area and their parameter distributions may not statistically meaningful.

These results show that the non-bedrock areas exhibit linear subsidence over a range of magnitudes up to -5 mm/yr and additionally, glaciofluvial and alluvial deposits exhibit a range of seasonal deformation values. InSAR deformation estimates allow for the spatial localization of those areas experiencing higher levels of deformation.

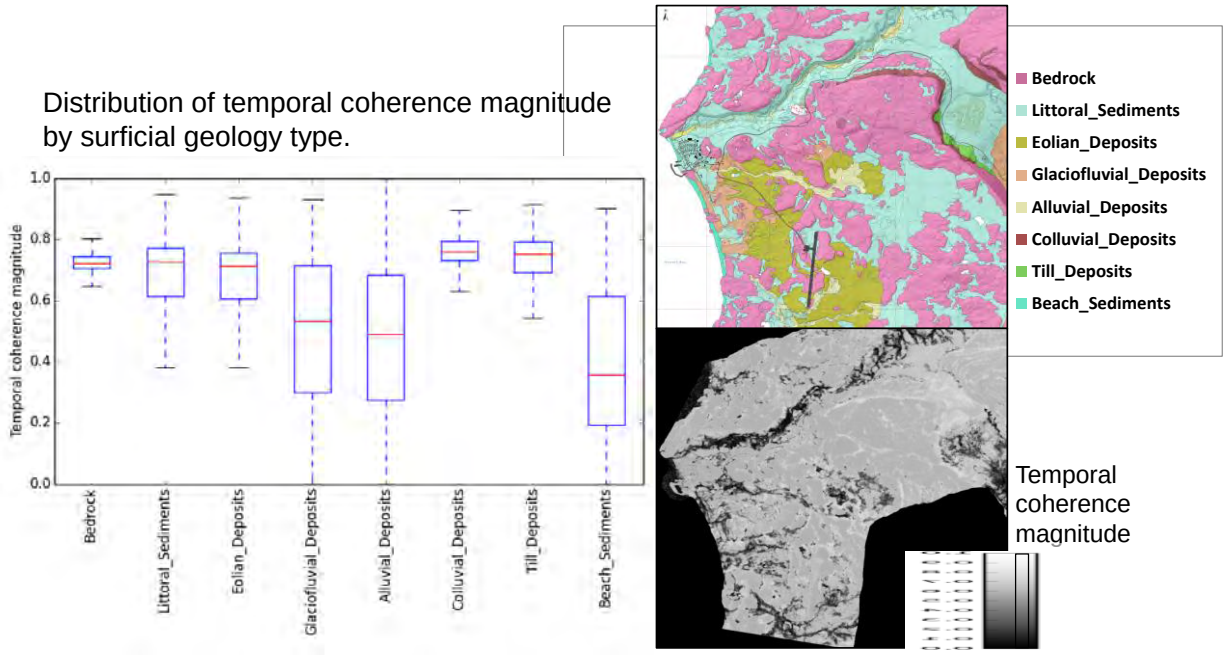

Figure 6-22 Umiujaq temporal coherence magnitude distribution boxplots according to surficial geology class. Note that the plotted whiskers extend 1.5 x the interquartile range.

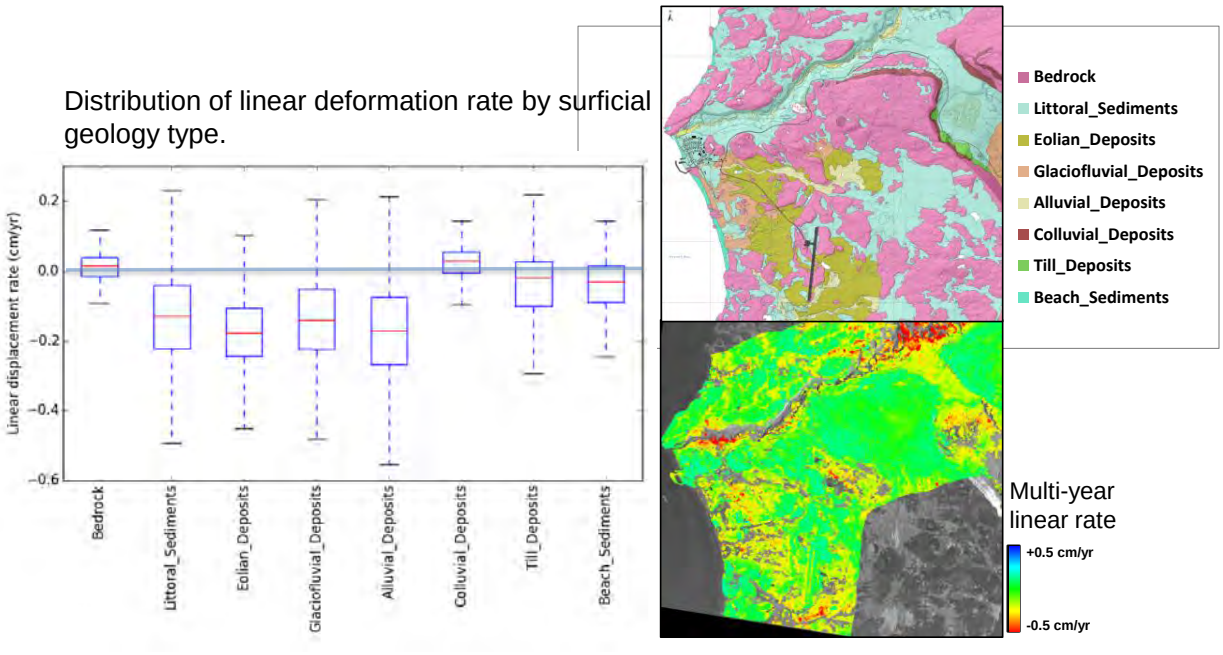

Figure 6-23 Umiujaq LOS linear deformation component distribution boxplots according to surficial geology class. Note that the plotted whiskers extend 1.5 x the interquartile range.

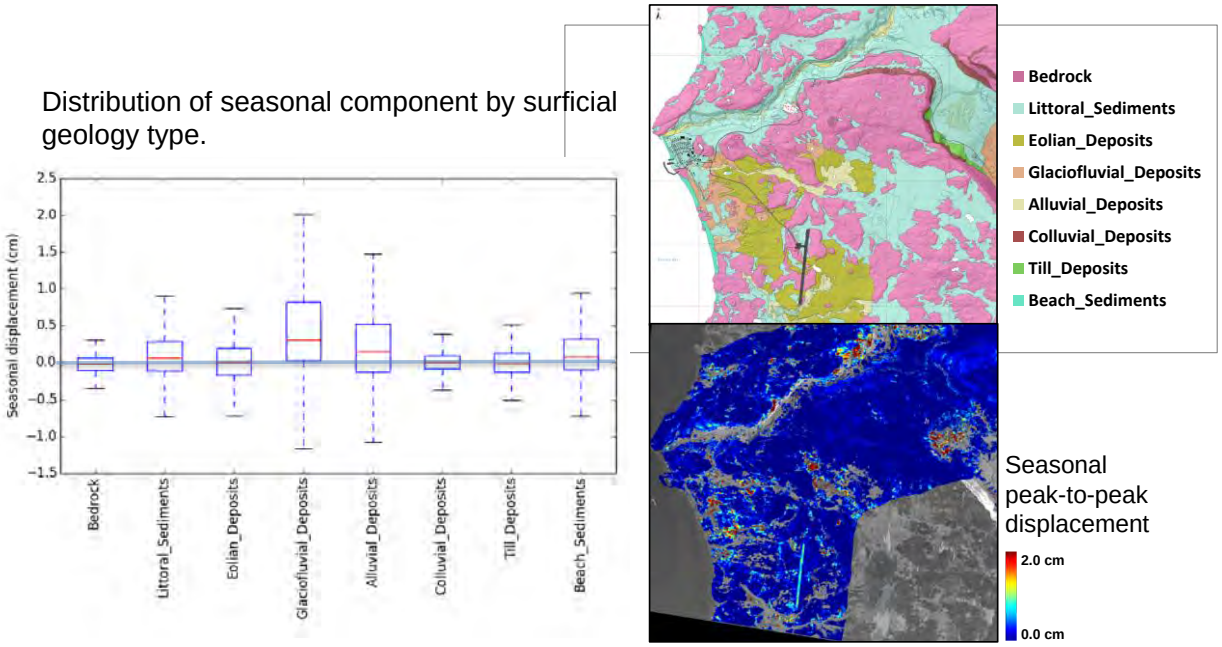

Figure 6-24 Umiujaq LOS seasonal deformation component distribution boxplots according to surficial geology class. Note that the plotted whiskers extend 1.5 x the interquartile range.

Figure 6-25 shows coherent target densities broken out by surficial geology class and by processing scenario. It should be noted that these densities are normalized by the number of looks used to generate each target since the processing method results in spatially oversampled samples. The normalization results in a density equivalent to the

number of independent samples per km^2. There is little variation observed between the four SLA scenarios and these show ~50 x10^3 targets/km^2 for bedrock, ~20 x10^3 targets/km^2 for littoral sediments and eolian deposits and ~5 x10^3 targets/km^2 for glaciofluvial and alluvial deposits. This results in a mean over the processed area of ~30 x10^3 targets/km^2). The largest variation within the SLA scenarios corresponds to the densities for the 2xSLA (summers) which are significantly lower for the littoral, eolian and glaciofluvial classes. This is likely due to the fact that the Multi-Track HDS InSAR processing results in a less accurate delineation of distributed targets than in the single stack cases and therefore the adaptive filtering applies a larger filter footprint. This reduces the spatial resolution of the result which leads to a lower density of independent targets. This effect is likely mitigated in the 3xSLA cases because it uses ~3x the number of scenes as are used in the 1xSLA case.

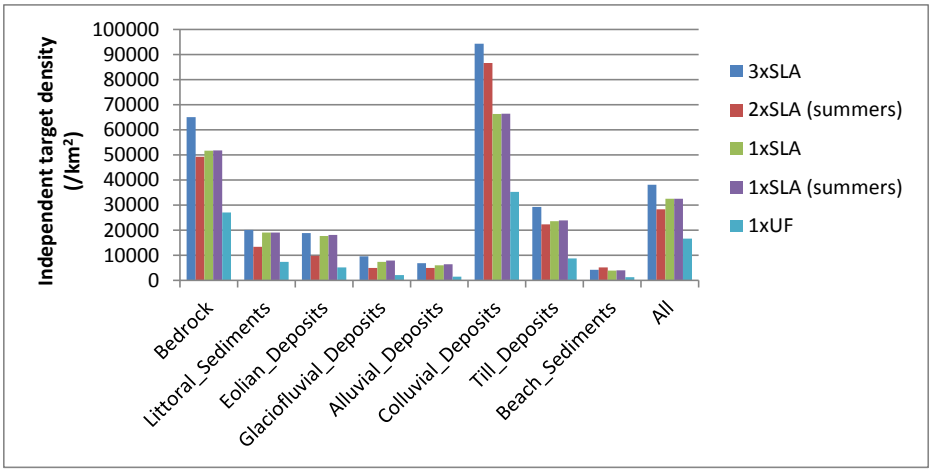

Figure 6-25 Umiujaq coherent target densities by surficial geology class and processing scenario.

6.3.4 Seasonal Cumulative Displacement

Dr. Michel Allard from CEN has suggested that it may be useful to render InSAR results as cumulative deformation maps corresponding to the full freeze/thaw periods. These maps cover time periods expected to correspond to the full freeze or thaw periods and therefore are intended to show the full seasonal deflection associated with these periods. This allows for a per-season view of the deformation estimates. It should be noted that these cumulative maps are sensitive to noise in the results since they are computed from only two deformation dates rather than the entire deformation history used for generating the linear and seasonal model components shown in the rest of this report. An example series of such maps for the Umiujaq RADARSAT-2 SLA Multi-Track HDS InSAR result is shown in Figure 6-26. There are many areas that show subsidence during the thaw periods and uplift during the freeze period. However there are other areas that show the opposite effect such as in the Tasiapik Valley and it is unclear whether these represent true deformation or are due to residual noise effects such as snow bias or uncorrected atmospheric phase.

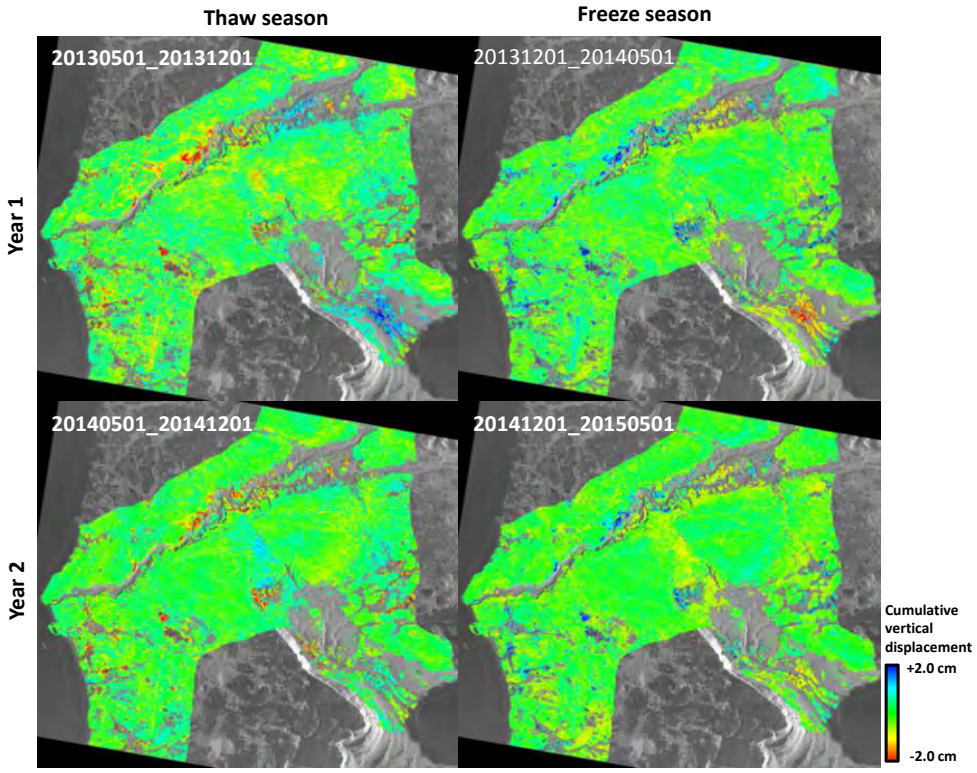

Figure 6-26 Cumulative seasonal deflection maps for Umiujaq generated using the three RADARSAT-2 SLA descending stacks.

6.4 Beaver Creek

Beaver Creek Multi-Track HDS InSAR deformation estimates were generated by processing two RADARSAT-2 descending spotlight stacks. InSAR image stacks used for this site are summarized in Figure 6-27, showing the image footprints and processed area and Table 6-5, which contains a summary of image parameters. The processing subset area was selected to include the highway and a relatively wide corridor on either side to reduce the likelihood of phase unwrapping issues through incoherent areas. This area includes the town of Beaver Creek at the northern end, a river crossing bridge near the centre and the highway test section near the southern end. The stacks cover a 27-month time period and include three snow free seasons.

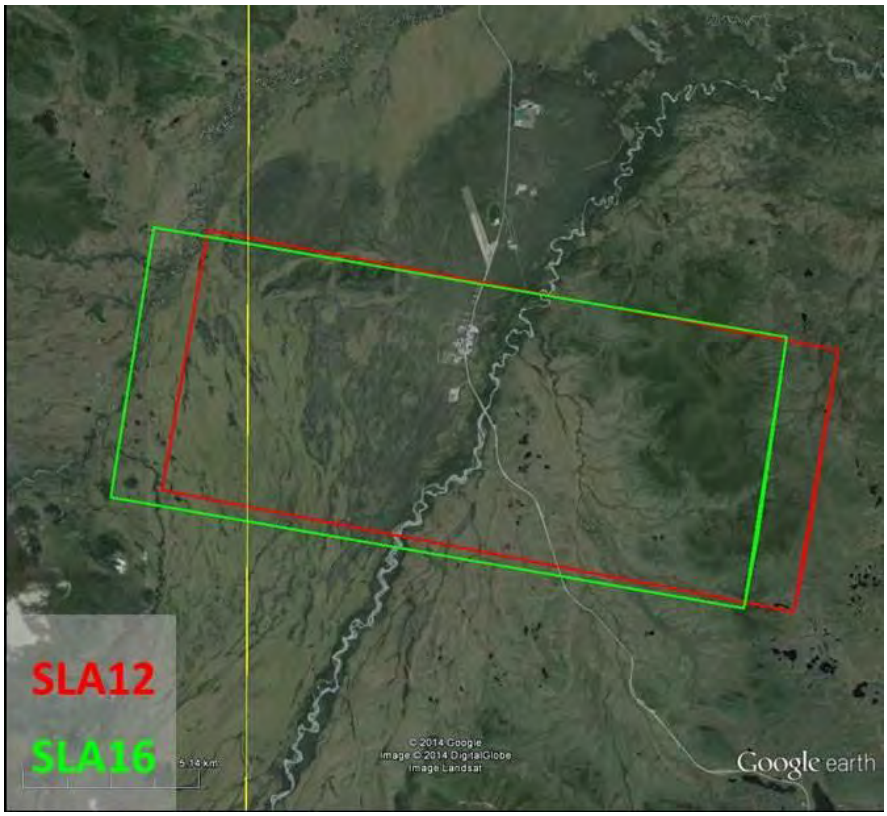

Figure 6-27 RADARSAT-2 data stacks processed over Beaver Creek

Table 6-5 RADARSAT-2 data processed for Beaver Creek

	Beam Mode	
	SLA12	**SLA16**
Number of scenes processed	34	35
Incidence angle	39.3º	42.1º
Processed data start date	2013-07-19	2013-07-26
Processed data end date	2015-10-13	2015-10-25

Figure 6-28 and Figure 6-29 show the linear and seasonal deformation component maps for the entire processed subset with inset areas highlighted. Coherent point coverage is generally good with the exception of the river and adjacent areas and the road surface south of the bridge which is known to have been resurfaced during the data acquisition period.

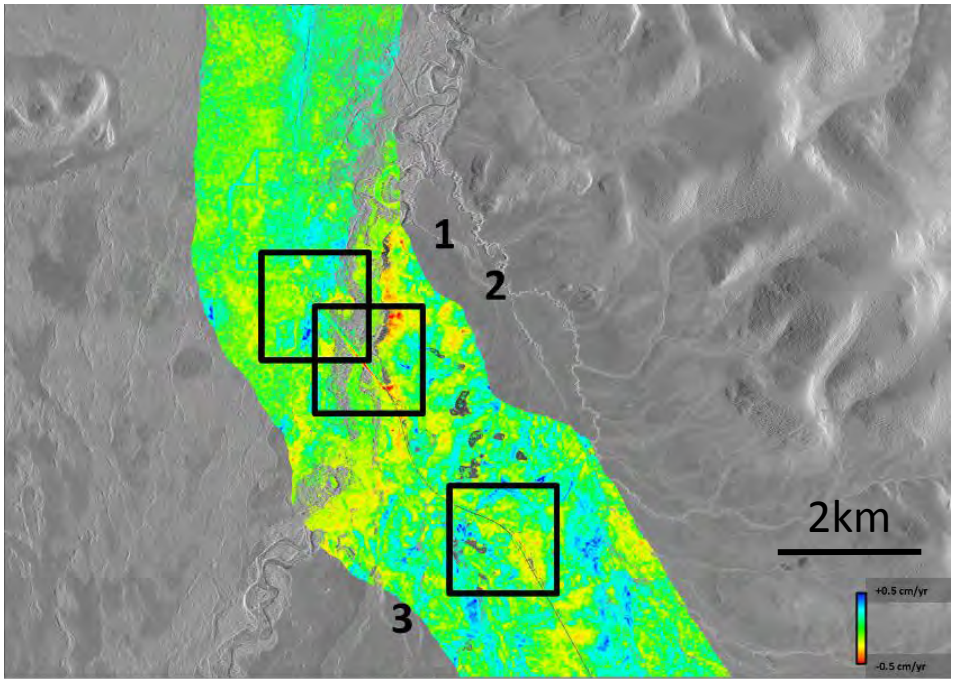

Figure 6-28 LOS linear deformation rate estimate over Beaver Creek with insets show for (1) highway north of bridge, (2) highway south of bridge and (3) testbed segment.

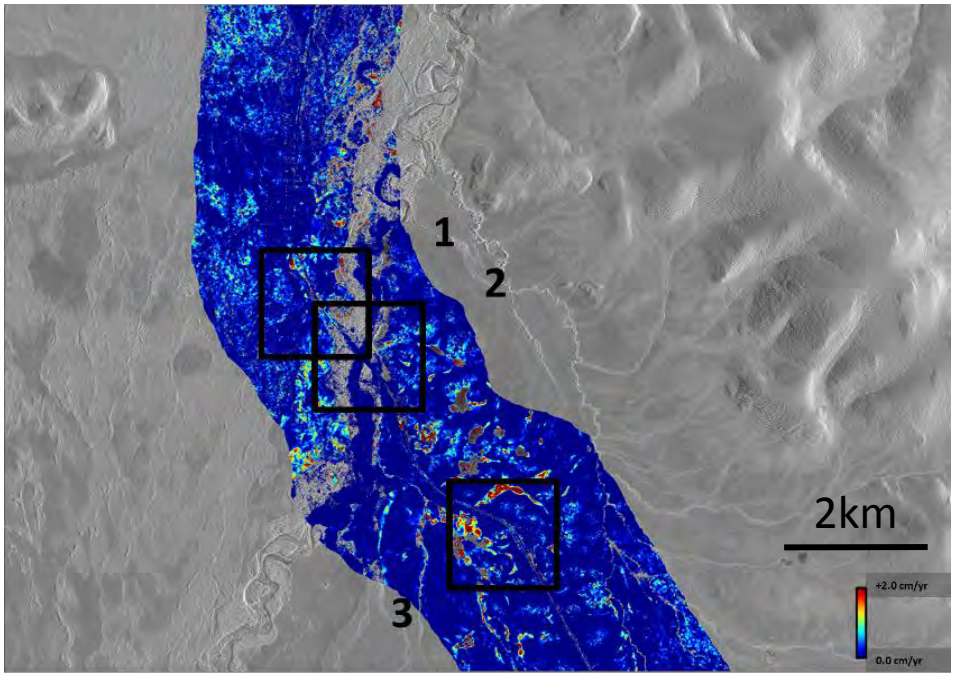

Figure 6-29 LOS seasonal motion amplitude estimate over Beaver Creek with insets show for (1) highway north of bridge, (2) highway south of bridge and (3) testbed segment.

Figure 6-30, Figure 6-31 and Figure 6-32 show deformation components for the inset areas. North of the bridge there are coherent targets on the road surface itself. There are no areas of significant linear deformation along this section. However there is significant variation in the seasonal deformation along this section. At the bridge itself the western embankment on either side appear to subside significantly. This in contrast with the eastern embankment which shows little deformation. This is likely due to the geometry of the descending LOS which is more sensitive to downslope movement on the western embankment. The area surrounding the highway test section shows many small areas of subsidence.

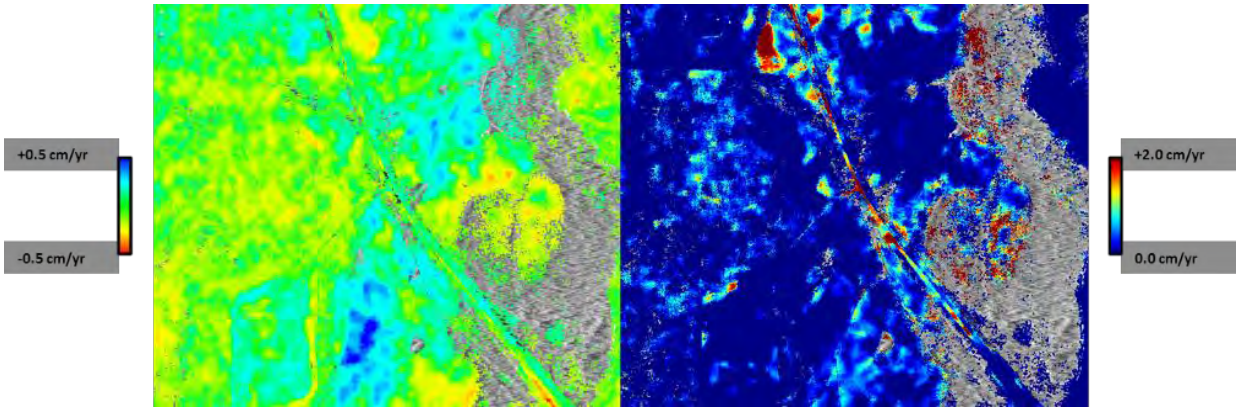

Figure 6-30 LOS linear deformation (left) and seasonal motion (right) over highway north of bridge.

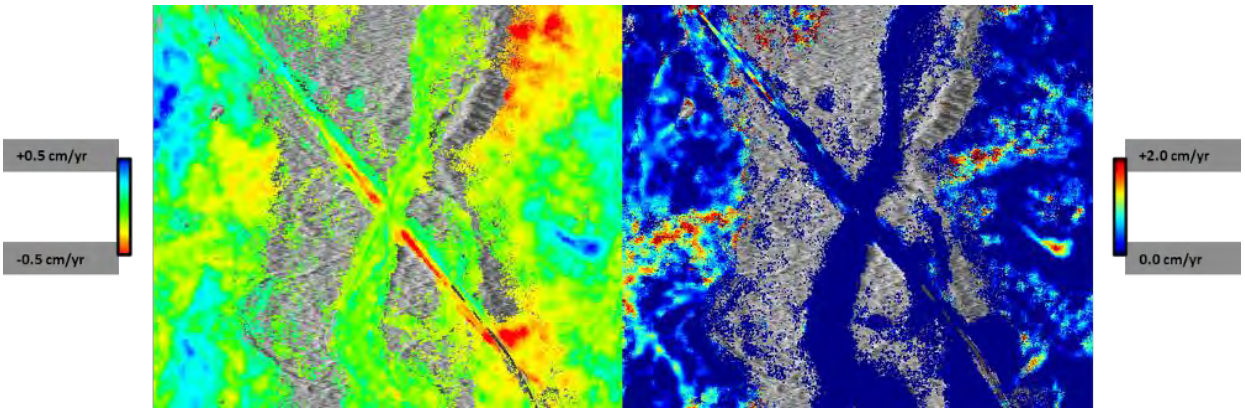

Figure 6-31 LOS linear deformation (left) and seasonal motion (right) over bridge area.

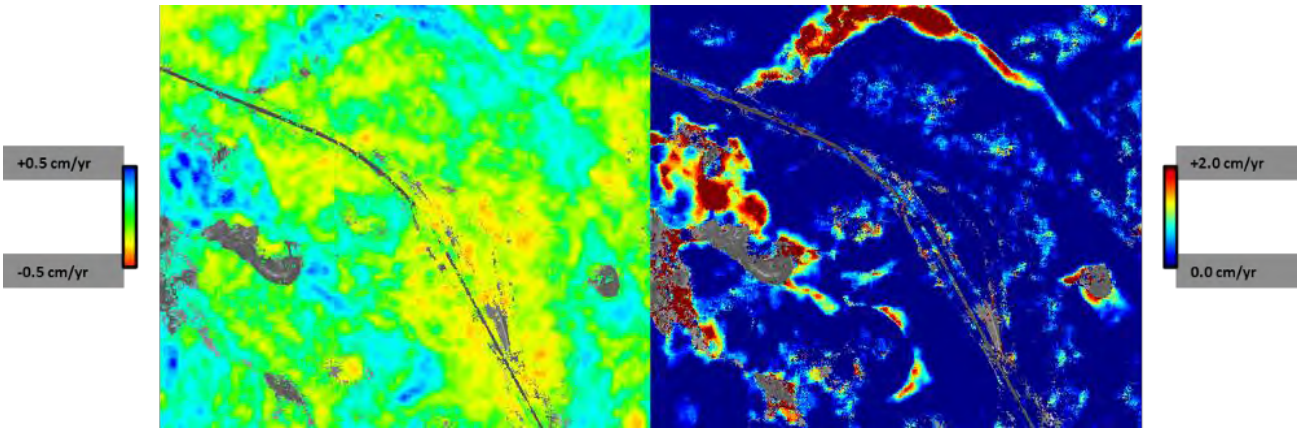

Figure 6-32 LOS linear deformation (left) and seasonal motion (right) over highway south of bridge that includes the highway test section.

Another area of significant subsidence is the slope just east of the highway and south of the bridge (Figure 6-33). This slope is immediately adjacent to a cut which also shows subsidence.

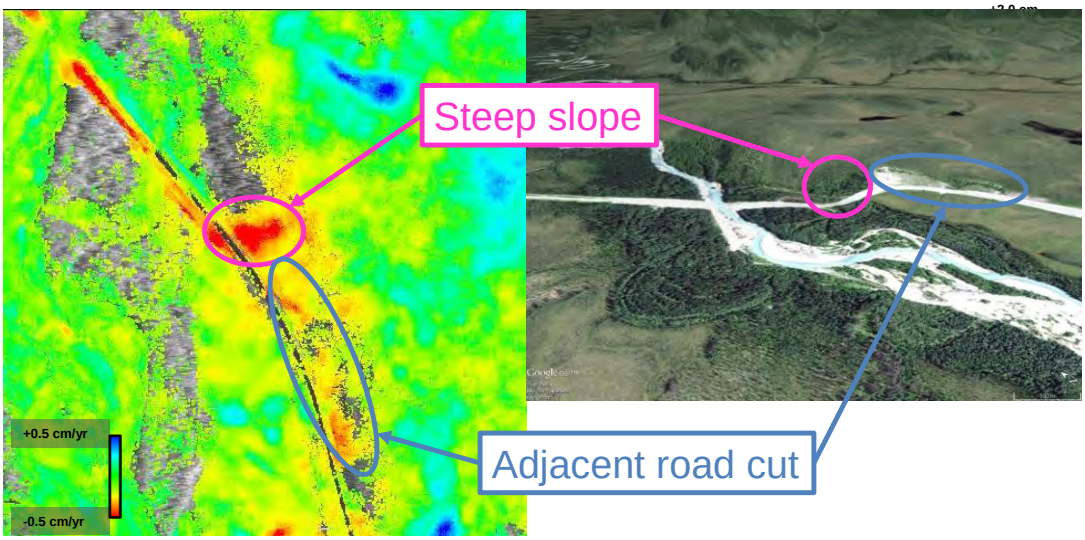

Figure 6-33 Deforming slope just south of bridge adjacent to road cut. A Google Earth optical image of the same area is shown on the right.

7 C-BAND/ X-BAND COMPARISON

A comparative analysis of C-/X-band InSAR results was conducted over the Umiujaq test site along with a demonstration of synergistic joint processing of C- and X-band data using Multi-Track HDS. Same side descending C- and X-band stacks were used from RADARSAT-2, TerraSAR-X, and COSMO-SkyMed. Table 7-1 below shows the data used for the analysis. Note that stack sizes were limited to achieve a comparable five month data window for each of the three sensors.

Table 7-1 Summary of SAR data stacks used in C-/X-band comparison

Sensor	Beam	Pass	Incidence Angle [°]	Ground Res [m]	Azimuth Res [m]	Swath [km]	Scenes	Start/End Dates
RS-2	SLA6	Des	34.7	2.8	0.8	18x8	5	2014/07 – 2014/10
RS-2	SLA15	Des	41.4	2.4	0.8	18x8	6	2014/06 – 2014/10
RS-2	SLA20	Des	44.8	2.3	0.8	18x8	6	2014/06 – 2014/10
TSX	HS24	Des	27.8	1.3	1.1	5x5	9	2014/06 – 2014/10
TSX	ST75	Des	48.1	0.8	0.2	4x4	9	2014/06 – 2014/10
CSK	SL12	Des	40.0	0.8	1.4	6x10	20	2014/06 – 2014/10

The temporal decorrelation for all the data was examined to determine the relative differences between C-band and X-band for Umiujaq which consists of sparsely vegetated tundra. In particular the ice bearing areas corresponding to the absence of surficial rock are of interest for permafrost monitoring. A mask was created based on the available surficial geology map over Umiujaq which removed surficial rock from the temporal decorrelation analysis.

For each stack the spatial coherence was estimated over a rectangular window. In order to minimize coherence estimation bias, a relatively large window of 21x21 was used for the lowest resolution stack and the windows for all other stacks were matched to have the same ground projected footprint. The resulting mean coherence is plotted below against temporal baseline for the three sensors in Figure 7-1. These results show similar decorrelation trends for TerraSAR-X and Cosmo-SkyMed and less decorrelation for RADARSAT-2 which is as expected given the sensors' carrier bands.

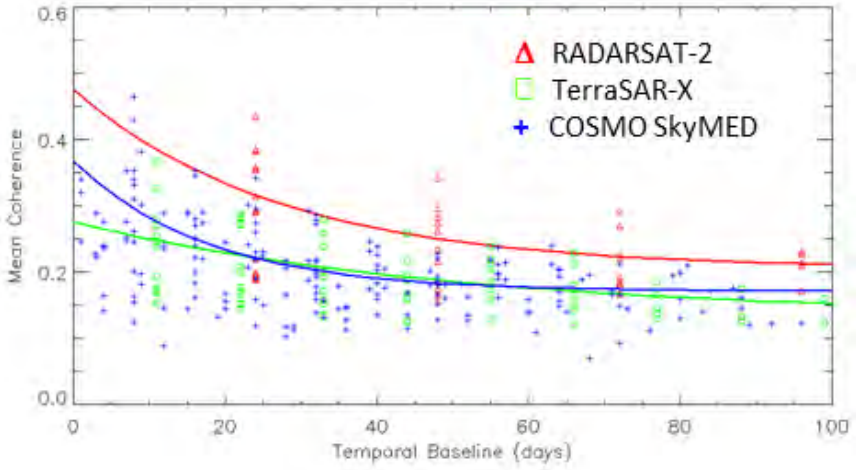

Figure 7-1 Sensor comparison of temporal decorrelation curves for non-rock areas. Solid curves correspond to coherence model fits to the estimates.

The stacks were combined using Multi-Track HDS InSAR in four separate combinations listed below in Table 7-2. The first three cases combine the available data for each sensor and the fourth case combines all the data for all sensors in a mixed-band case.

Table 7-2 Summary of SAR data stacks used in test cases

Test Case	Stacks Included	Number of Scenes	Number of Interferograms
RADARSAT-2	RS2_SLA6/RS2_SLA15/RS2_SLA20	17	40
TerraSAR-X	TSX_HS24/TSX_ST75	18	72
COSMO-SkyMed	CSK_SL12	20	190
All Sensors	RS2_SLA6/RS2_SLA15/RS2_SLA20 TSX_HS24/TSX_ST75/CSK_SL12	55	302

The time period studied for all the cases is from June to October (corresponds to span of CSK dataset) and represents primarily the active layer thaw phase. Deformation in this phase is approximately linear over the period being analyzed and is not readily separable from long-term deformation. Therefore only the seasonal motion component was fit to the data. The vertically projected seasonal deformation magnitude maps for the four test cases along with the surficial geology are shown below in Figure 7-2. The maps show similar spatial coverage with the ALL case having the best coverage of coherent targets. The maps show similar deformation patterns although some differences can be observed.

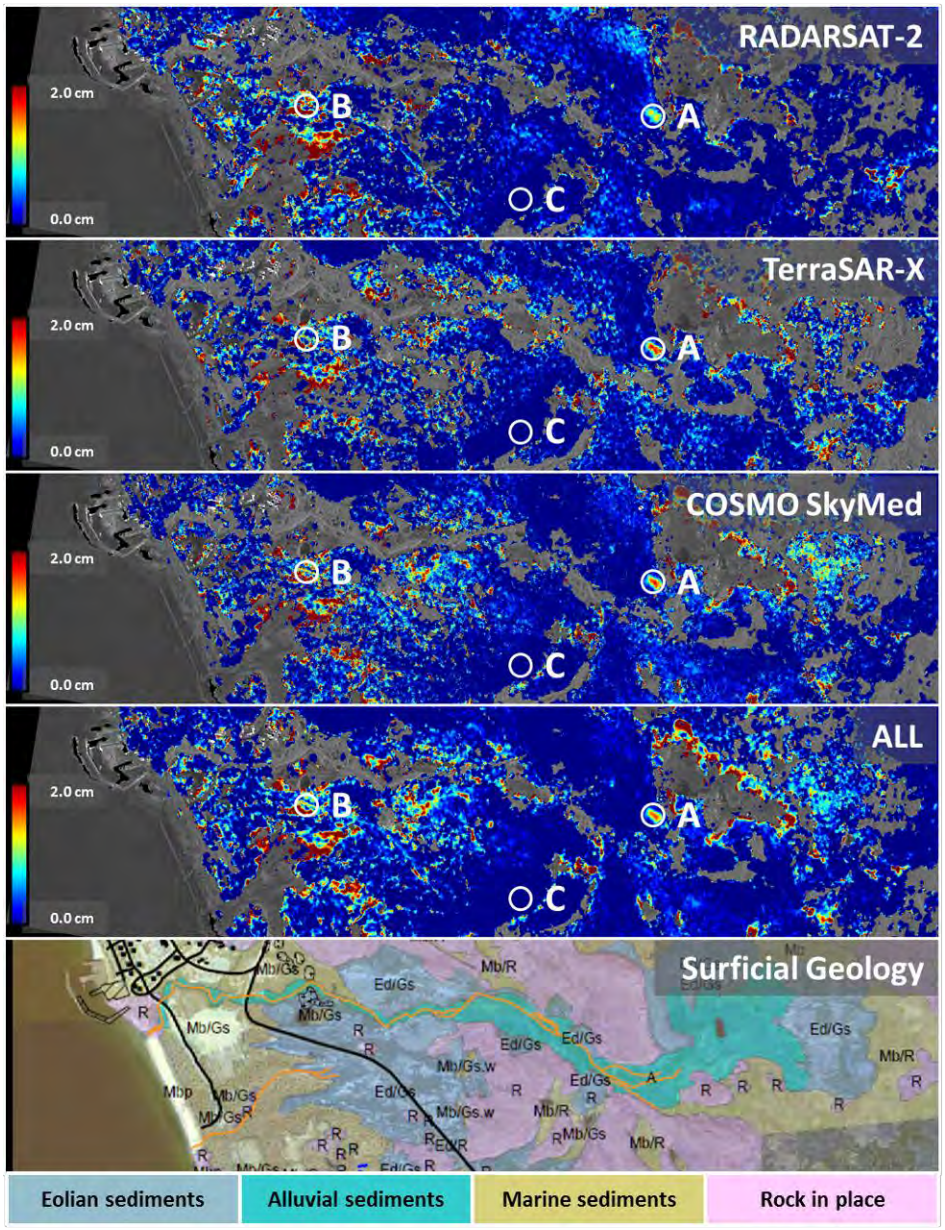

Figure 7-2 Seasonal deformation maps along with the corresponding surficial geology

Comparison with the surficial geology shows a good degree of correlation between areas of low seasonal deformation magnitude and areas of surficial rock. Incoherent areas also correlate well with areas of marine and alluvial sediments. In the area west of point B there is a reasonable correlation between marine sediments and higher seasonal deformation magnitudes.

8 ALTERNATE SCENARIOS

As part of the final project assessments, we investigated the sensitivity of the InSAR deformation estimates to changes in temporal sampling and spatial resolution. The final analysis results reported for Umiujaq, Salluit and Beaver Creek were generated using multiple spotlight mode data stacks per site. These results represent a high sampling rate scenario both temporally, as provided by jointly processing multiple stacks and spatially by using the highest resolution modes available. One obvious question that arises is whether results providing similar utility for infrastructure monitoring can be obtained with fewer SAR acquisitions or using modes with lower spatial resolution but wider spatial coverage. Results from this analysis provide useful information for planning cost effective monitoring strategies over potentially extended infrastructure.

Alternate processing scenarios for Umiujaq and Beaver Creek were constructed as combinations of the following:

1. Number of stacks used: fewer stacks jointly processed correspond to a simple reduction in the temporal sampling rate
2. Use of summer only scenes: winter scenes are more affected by snow related phase bias and therefore may do less to improve the accuracy of the deformation estimates than summer scenes.
3. Using lower resolution modes: Comparing RADARSAT-2 Spotlight mode (~1.5 m resolution, 144 km^2/scene) results with Ultra-fine (~3 m resolution, 400 km^2/scene) and Multi-look Fine (~5 m, 2500 km^2/scene).

8.1 Umiujaq

Five scenarios for Umiujaq were investigated and are summarized in Table 8-1. The first four scenarios all use RADARSAT-2 spotlight stacks but vary the number of stacks used and whether the non-summer scenes are included in the analysis. The fifth scenario uses a single RADARSAT-2 Ultra-fine stack and therefore should be compared to the 1xSLA scenario to examine the impact of the lower spatial resolution.

Table 8-1 Alternate scenarios investigated for Umiujaq site.

Scenario	Stacks	Number of scenes	Time period	Nominal Resolution (m)	Description
3xSLA (gold standard)	SLA6, SLA15, SLA20	105	07/2013 – 10/2015	1.5	All spotlight scenes.
1xSLA	SLA6	33	08/2013 – 10/2015	1.5	Single spotlight stack.
2xSLA (summers)	SLA6, SLA15	33	08/2013 – 09/2015	1.5	Two spotlight stacks, summer data only.

Scenario	Stacks	Number of scenes	Time period	Nominal Resolution (m)	Description
1xSLA (summers)	SLA6	16	08/2013 – 09/2015	1.5	Single spotlight stack, summer data only.
1xUF	U1	31	08/2013 – 10/2015	3.0	Single Ultra-fine stack – lower resolution.

Linear deformation estimate maps for the five scenarios are shown in Figure 8-1. These show very similar large scale spatial patterns of subsidence. However there are differences in the spatial coverage and density of coherent targets and also in the estimated deformation magnitudes. Spatial maps of the difference between the 3xSLA (treat as a gold standard) and the four alternate scenarios for the linear and seasonal deformation components are shown in Figure 8-2 and Figure 8-3. RMS parameter difference statistics and mean target densities per square kilometer are listed in Table 8-2. These results show that for estimation of linear estimation all three alternate SLA scenarios produce similar results. However the UF scenario shows larger differences which may be due to higher phase noise resulting from less multi-looking compared to the SLA scenarios. For estimation of the seasonal component, the summer only scenarios show greater differences with respect to the gold standard which suggest that winter scenes are necessary to quantify the full seasonal deformation component.

Coherent target coverage is highest for the 3xSLA scenario and lowest for the 1xUF scenario. However, the 2xSLA (summers only) scenario has nearly as complete coverage as the 3xSLA scenario with only ~1/3 the number of scenes used.

On the runway, coherent targets are only retained in the scenarios with winter scenes. The runway is unpaved and therefore this may be due to the fact that runway coherence is lower over the summer months due to surface disturbance resulting from airport operations.

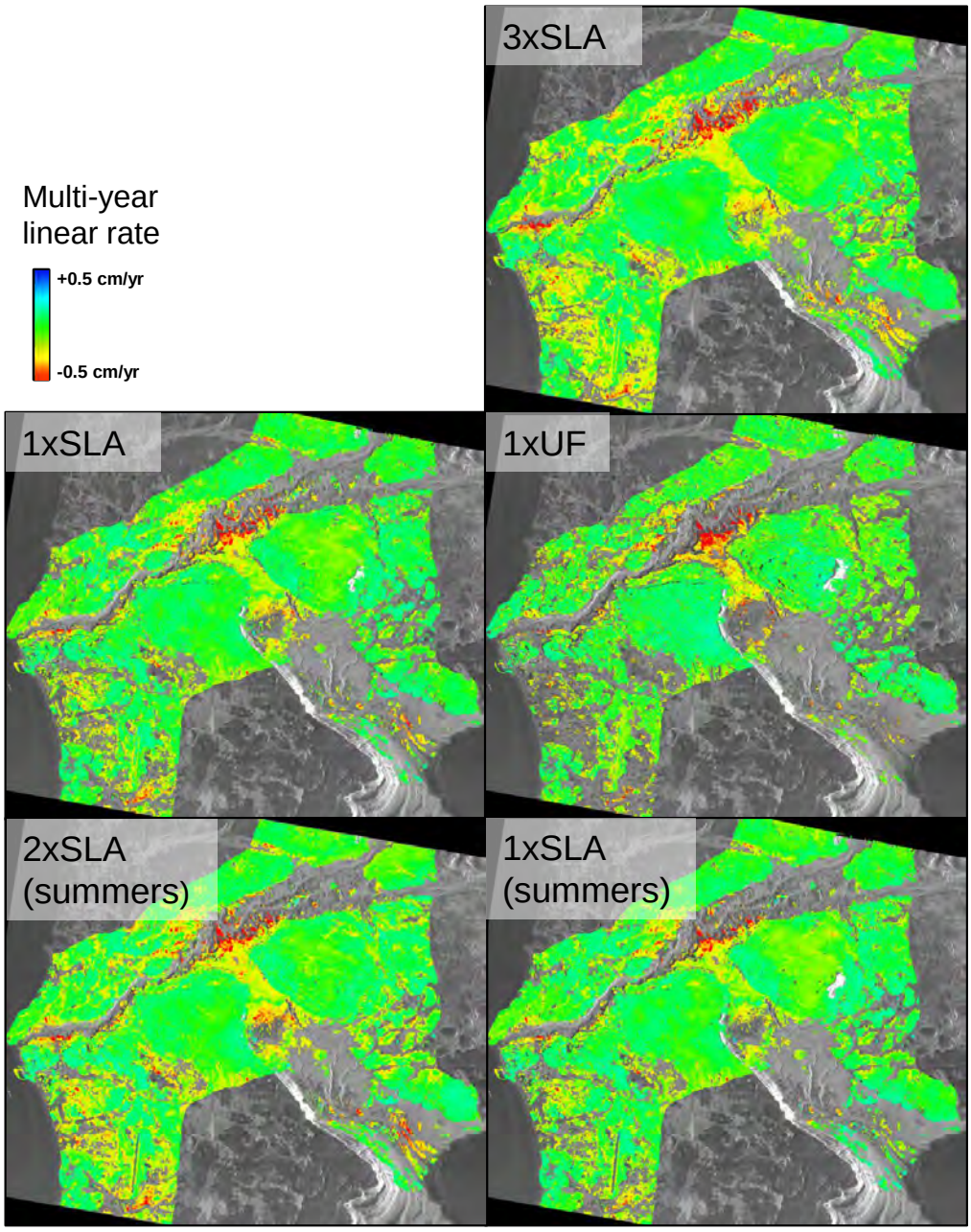

Figure 8-1 Linear deformation rate maps for the five Umiujaq scenarios.

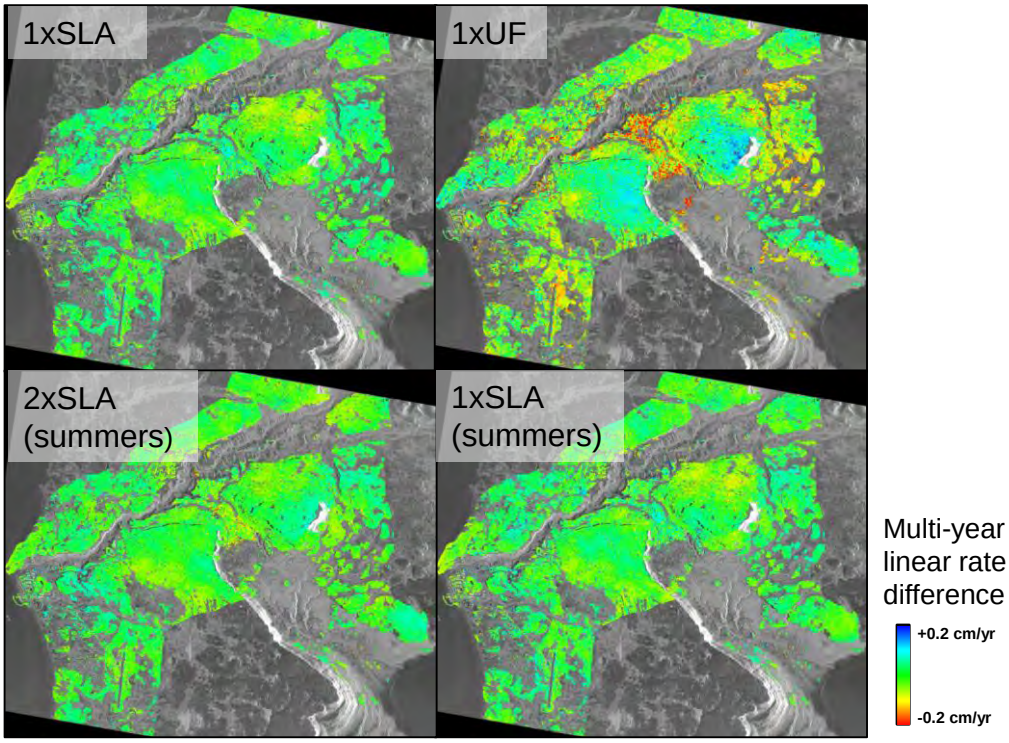

Figure 8-2 Umiujaq linear deformation rate difference maps comparing the four alternate scenarios to the gold standard scenario.

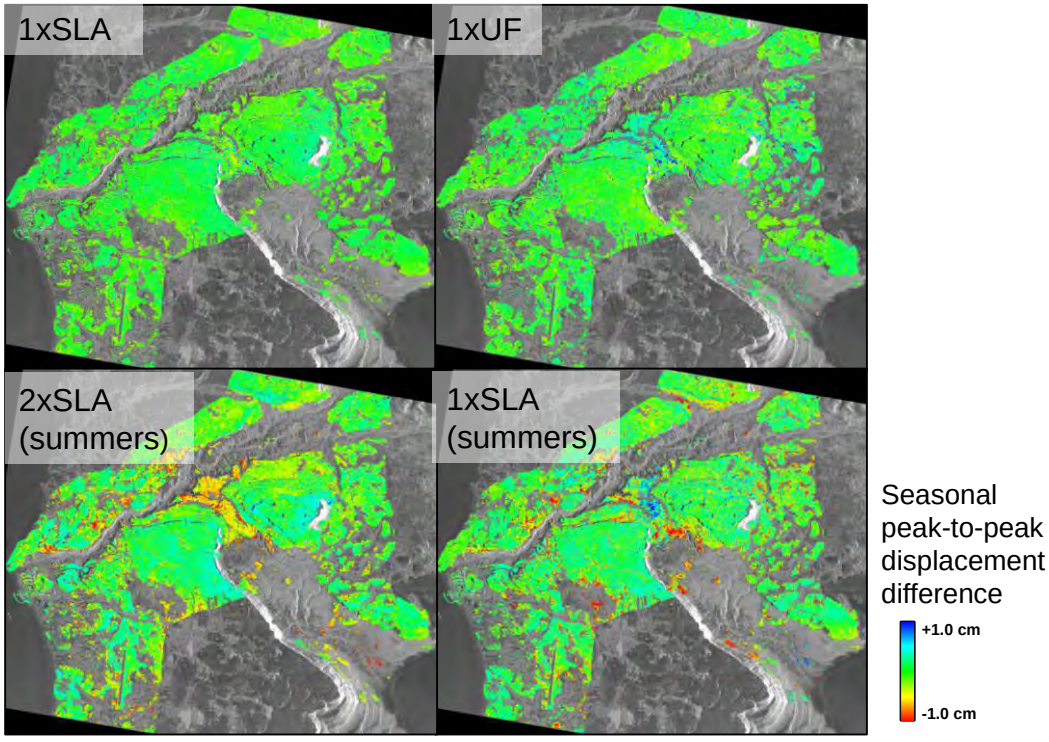

Figure 8-3 Umiujaq seasonal peak-to-peak displacement difference maps comparing the four alternate scenarios to the gold standard scenario.

Table 8-2 Summary of results for alternate scenarios investigated for Umiujaq site.

Scenario	Stacks	Number of scenes	Oversampled target density (10^3 pts/km^2)	RMS Linear rate difference (cm/yr)	RMS Seasonal component difference (cm)
3xSLA (gold standard)	SLA6, SLA15, SLA20	105	198	-	-
1xSLA	SLA6	33	135	0.042	0.18
2xSLA (summers)	SLA6, SLA15	33	186	0.036	0.31
1xSLA (summers)	SLA6	16	136	0.049	0.38
1xUF	U1	31	123	0.080	0.24

8.2 Beaver Creek

Three scenarios for Beaver Creek were investigated and are summarized in Table 8-3. The two alternate scenarios investigate using single stacks of either SLA or MF mode data.

Linear deformation estimate maps for the three scenarios are shown in Figure 8-4. Spatial maps of the difference between the 2xSLA (treat as a gold standard) and the two alternate scenarios for the linear and seasonal deformation components are shown in Figure 8-5 and Figure 8-6. RMS parameter difference statistics and mean target densities per square kilometre are listed in Table 8-4. These show nearly identical results between the 1xSLA and 2xSLA scenarios both in terms of coherent target coverage and also it terms of the deformation model parameter values.

However significant differences are observed between the 1xMF and both SLA scenarios including significantly sparser target coverage and significant differences in the linear and seasonal deformation estimates which are likely due to a combination of the lower spatial resolution and reduced phase noise suppression resulting from less multi-looking. These results indicate that MF despite having significantly more spatial coverage per scene, provides a much less complete picture of the deformation occurring along the highway corridor.

Table 8-3 Alternate scenarios investigated for Beaver Creek site.

Scenario	Stacks	Number of scenes	Time period	Nominal Resolution (m)	Description
2xSLA (gold standard)	SLA12, SLA16	71	07/2013 – 10/2015	1.5	All spotlight scenes.

Scenario	Stacks	Number of scenes	Time period	Nominal Resolution (m)	Description
1xSLA	SLA12	35	07/2013 – 10/2015	1.5	Single spotlight stack.
1xMF	MF22N	33	08/2013 – 09/2015	5.0	Single Multi-Look fine stack – lower spatial resolution.

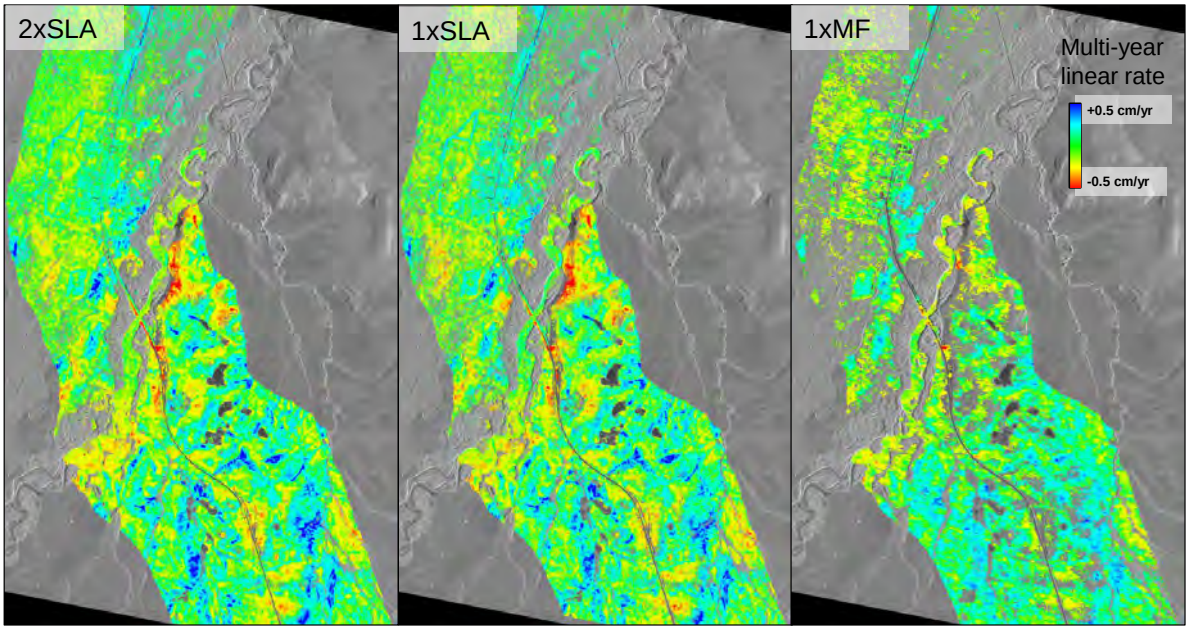

Figure 8-4 Linear deformation rate maps for the three Beaver Creek scenarios.

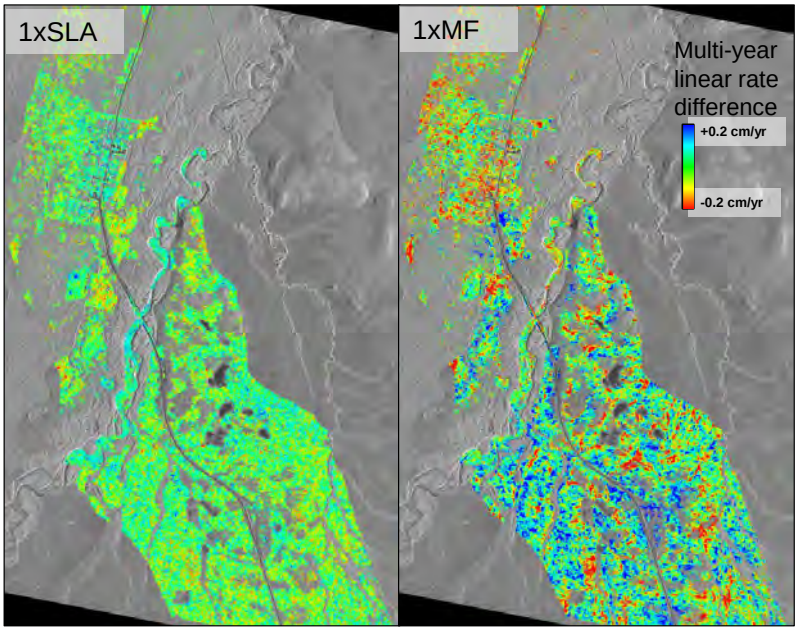

Figure 8-5 Beaver Creek linear deformation rate difference maps comparing the two alternate scenarios to the gold standard scenario.

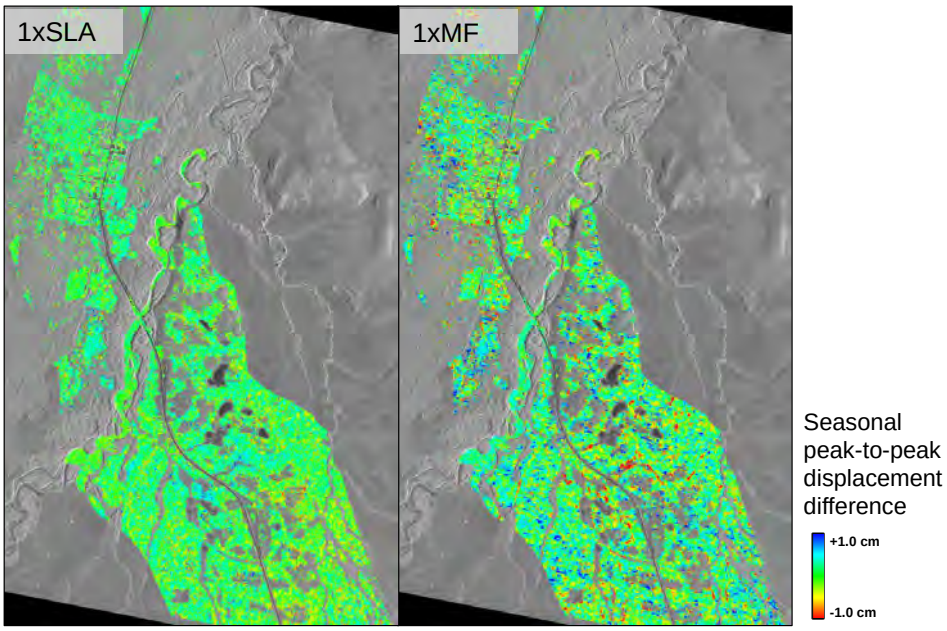

Figure 8-6 Beaver Creek seasonal peak-to-peak displacement difference maps comparing the two alternate scenarios to the gold standard scenario.

Table 8-4 Summary of results for alternate scenarios investigated for Beaver Creek site.

Scenario	Stacks	Number of scenes	Oversampled target density (10^3 pts/km^2)	RMS Linear rate difference (cm/yr)	RMS Seasonal component difference (cm)
2xSLA (gold standard)	SLA12, SLA16	71	207	-	-
1xSLA	SLA12	35	201	0.084	0.38
1xMF	SLA6, SLA15	33	64	0.138	0.56

9 CONCLUSIONS AND RECOMMENDATIONS

9.1 Conclusions

This project has involved the development of an enhanced Multi-Track HDS InSAR solution that has focused on addressing specific challenges posed by monitoring infrastructure in permafrost affected areas. The developed solution has been tested over multiple sites within northern Canada with SAR data stacks from RADARSAT-2 as well as the TerraSAR-X and COSMO-SkyMed X-band sensors. Multiple processing scenarios have been investigated to assess the best monitoring strategies to minimize monitoring costs.

An assessment of the results with respect to the performance indicators identified at the beginning of the project is given below:

PI1: Evaluate AO and Team capabilities and needs, available data and solution requirements to select sites that provide suitable testing environments and scenarios to support project objectives and algorithm development.

Sites were selected in order to meet multiple project objectives. These include:

- existence of multiple infrastructure types of interest for monitoring, most notably: highways and roads with a variety of surface treatments (asphalt, gravel, chip seal), buildings, bridges and airstrips
- variety of terrain types: slopes, alluvial valleys, coastal areas
- variety of surficial geology types: surficial rock, till, sediments etc.
- existence of periglacial landforms and features
- discontinuous or sporadic permafrost areas expected to be susceptible to surface deformation resulting from permafrost changes
- sites directly supported by project partners at CEN
- sites involving multiple government jurisdictions in northern Canada to provide the opportunity to work with and receive feedback from multiple end-user groups
- at least one site with sufficient archive data to allow method development prior to maturation of prospectively acquired data stacks

The selected set of sites (Umiujaq, Salluit, Beaver Creek, Inuvik and Yellowknife) meet all of these objectives and have allowed the development and assessment of an InSAR based monitoring solution that should be applicable to a broad range of monitoring applications in permafrost affect areas.

PI2: Conduct field visits to the sites at Salluit and Umiujaq to collect ground truth and ancillary data and to install CRs.

CEN conducted multiple field visits to both the Salluit and Umiujaq sites during the project. At Umiujaq that included installation and inspection of the floating and anchored CRs as well as installation and periodic measurement of scratch gauges installed at the anchored CRs. The site visits also included inspection and photography of areas observed by InSAR to exhibit surface deformation. These include both infrastructure and natural features.

PI3: Develop a novel high temporal resolution version of MDA's advanced Homogenous Distributed Scatterer InSAR. (Multi-Track InSAR)

Considerable work was done to implement and enhance the proposed Multi-Track HDS InSAR solution. Prior to the project an initial implementation of this solution had been implemented as a proof of concept but with several major shortcomings including difficulty for a skilled operator to use routinely, corruption of phase values, loss of spatial resolution, geocoding errors and burdensome computational performance. All of these were addressed during the project resulting in a much easier to use solution that is capable of yielding precise deformation estimates from multiple same-side geometry data stacks. These improvements have been demonstrated in side-by-side comparisons of outputs generated by the initial and refined solutions.

This solution enables the rapid acquisition of a SAR dataset with sufficient number of scenes to perform multi-temporal InSAR analysis.

PI4: Develop a system to generate permafrost-type classification and risk assessment maps from the seasonal and long-term permafrost displacement products.

The solution developed during this project provides multi-temporal surface deformation estimates for infrastructure (roads, buildings, storage tanks, bridges, embankments, airstrips) and natural terrain including a variety of surficial conditions. These estimates consist of a time-series of deformation maps allowing the generation of cumulative deformation maps between any two points in time within the monitoring period. These estimates allow for the plotting of deformation time series for any coherent point within the processed area. This allows for detailed analysis of the temporal behavior of any point of interest provided that is coherent.

The estimates also may be used to constrain a parametric deformation model for each spatial point which allows for the separation of long term linear trends from seasonal deformation. This approach was used during the project to generate seasonal and linear deformation maps of the study site.

The ability to separate linear and seasonal deformation is important because it is the linear component that, over time, can pose a greater risk to infrastructure since it results in ever increasing strains which may exceed infrastructure design limits.

There are several areas within the Umiujaq processed area containing lithalsas that were not well characterized by the InSAR deformation estimates. These very active and relatively small palsas present a significant challenge for InSAR monitoring and could be addressed through future solution improvements.

PI5: Perform a comparison analysis of MDA's InSAR solution using C-band and X-band SAR data.

Work was done to allow for processing both TerraSAR-X and COSMO-SkyMed data with the Multi-Track HDS InSAR solution. A direct comparison of the solution using RADARSAT-2, TerraSAR-X and COSMO-SkyMed data over the Umiujaq test site was performed for the same 100 day time period during the summer 2014. Side-by-side comparison of the generated deformation outputs showed substantial similarity for each sensor individually and in combination. These results demonstrate that the Multi-Track HDS InSAR solution can be used for deformation monitoring of permafrost areas with either C- or X-band data. The solution also allows interleaving SAR data stacks from different sensors including from different carrier bands which allows for potential mitigation of satellite failure through redundant acquisition by multiple sensors.

An analysis of temporal decorrelation times for the three sensors over non-bedrock areas within the Umiujaq processed area estimated that C-band decorrelation at 24-day repeat intervals is similar to that which occurs over ~7 days for X-band. This confirms that the decorrelation experienced by RADARSAT-2 (24 day repeat) compares favourably to that experienced by either TerraSAR-X (11 day repeat) or COSMO-SkyMed (4-day mean repeat over constellation).

PI6: Demonstrate and assess the potential of the service and recommend the next steps for its operationalization.

Multi-temporal InSAR deformation estimates were generated for the Salluit, Umiujaq, Beaver Creek and Yellowknife test sites. In all cases the spatial coverage of coherent targets was very good in most areas within the processed areas of interest. Alternate dataset scenarios were investigated to determine whether comparable estimated could be generated with less data. This work showed that reasonable estimates of linear deformation can be obtained with single data stacks and with summer only acquisitions. For example a single stack of 16 summer-only acquisitions was used to generate a reasonable characterization of linear deformation over the study area.

An analysis of the impact of spatial resolution showed that spatial coverage and estimation precision are better with higher resolution data. This effect is a trade-off with the wider spatial coverage that comes with coarser resolution modes. One potential option is the use of wide mode RADARSAT-2 data such as Ultra-fine Wide which provides 50 km swath coverage and 3m resolution at the cost of higher quantization noise.

9.2 Contractors Evaluation of Overall Success of the Project

Surface deformation caused by changing permafrost conditions poses a threat to existing and planned infrastructure in many areas within the Arctic and sub-Arctic. Satellite based synthetic aperture radar interferometry (InSAR) is a method that measures surface deformation at continuously repeating intervals over wide spatial scales. This provides quantification of ongoing change and also has the potential to map areas at risk of future change by characterizing the surface expression of seasonal changes to the permafrost active layer.

Robust monitoring of permafrost areas with InSAR is faced with several challenges related to the temporal and spatial characteristics of the measured deformation. Seasonal snow cover reduces coherence over many months of the year and results in wide scale phase biases. Complex deformation dynamics arise due to the combination of seasonal active-layer induced heave and long term subsidence caused by permanent changes in ice content. Spatial variability in permafrost conditions can result in high spatial phase gradients which make phase unwrapping difficult.

The Multi-Track HDS InSAR solution developed during the project is designed to provide sufficient spatial and temporal sampling to adequately characterize the surface deformation in areas of high spatial phase gradients. This method jointly processes multiple same-side SAR data stacks from one or more sensors which improves the achievable temporal sampling rate. Spatial resolution is preserved while supressing phase noise by the use of spatially adaptive multi-looking. The method also includes a model for the surface expression of seasonal active layer changes which improves phase unwrapping and provides means for quantifying the seasonal deformation. This allows for more accurate estimation of long term deformation using a shorter observation window.

The results obtained by applying the solution to the project test sites confirm that it does provide deformation monitoring with sufficiently high spatial coverage and resolution to monitor both infrastructure and most areas of natural terrain. This coverage is highest in areas of surficial rock which typically do not pose risks to infrastructure. However the coverage for other potentially ice bearing surficial geology types was also found to be sufficiently high to allow robust monitoring in many cases.

Both spatial coverage and precision of deformation estimates was found to be best with spotlight mode data. For the RADARSAT-2 case it is recommended to use spotlight mode data for monitoring compact/high value areas such as villages or industrial areas. For wide scale monitoring applications such as highway monitoring it is suggested that the use of Ultrafine Wide mode be investigated since it provides 50 km swath width and 3 m spatial resolution.

The use of Multi-Track HDS has been demonstrated to allow rapid accumulation of viable datasets within a single summer season and to allow for the combination of data from different sensors and even different carrier bands. However it should be noted that if the goal is to estimate long term ‘linear’ deformation without undue bias from the

seasonal deformation caused by the active layer freeze/thaw cycle then multiple years of data (i.e. including two or more snow free seasons) are needed. In such cases it has been shown that reasonable deformation estimates can be obtained from a single data stack with only marginal benefit gained from adding additional data stacks. Reasonable estimates of linear deformation may be obtained using only summer acquisition which further reduces data requirements. However, if the goal is also to map the amplitude of seasonal deformation, then it is preferable to include winter acquisitions in the analysis.

Feedback from territorial transportation managers involved with the project has been favourable regarding the developed solution's potential. They have indicated that InSAR products provide information useful to transportation groups for advance planning of areas requiring permafrost mitigation or remediation and as useful inputs for route selection for new infrastructure or when rehabilitating existing infrastructure. They have stated that the year-to-year linear deformation product is generally sufficient for their needs and that seasonal deformation may be useful on a more limited basis. One concern raised is the issue of data access (i.e. data planning, collection and dissemination within current NMSO allocations) and its impact on the operational viability of an InSAR based solution.

Permafrost scientists involved in the project have stated that InSAR products provide spatial information on surface movements consistent with permafrost seasonal movements and thaw/degradation. The high spatial resolution surface movement information provided by the InSAR solution is consistent with and supports information used by permafrost scientists through analysis of surficial geology or ground surveys and occasionally provides information on movement that is not readily observable by other means. They have also indicated that having access to contextual information leads to improved interpretation of the InSAR products.

These favourable results and end-user feedback support the assertion that the developed solution has considerable potential to support the establishment of a commercial InSAR based solution for infrastructure monitoring in permafrost affected areas. The C-/X-band comparison results indicate that a commercial solution could exploit data from both C- and X-band SAR sensors. This has the benefit of offering increased temporal coverage and data availability compared to that which could be achieved with a single sensor or sensor constellation.

A DEVELOPED AND DELIVERED SOFTWARE TOOLS

A1 System Requirements

A1.1 Hardware

The Foreground Intellectual Property (FIP) modules provided for this project were run on a RHEL based Linux operating system. Due to the computationally-intensive procedures, the processor should have a minimum of 4 cores, 8 GB of RAM, and storage capacity of at least 4 TB.

A1.2 Software

Nearly all software modules developed for this project were coded in IDL, version 6.4. IDL is a data visualization programming language commercially available from Exelisvis (http://www.exelisvis.com/ProductsServices/IDL.aspx). An IDL license (version 6.4 or higher) is required in order to run the provided FIP code and to load the MDA Background Intellectual Property (BIP) modules.

BIP required to run FIP

IDL .sav files
The MDA BIP modules required to run the FIP modules are delivered as IDL .sav files containing compiled IDL procedures and functions. These .sav files can be loaded from an IDL terminal.

Colortables
MDA's renderings are generated using ASCII colortables. These have been provided in the colortables folder and the folder must be added to the user's IDL path (IDL_PATH).

Third-party software required to run FIP and BIP modules

This section includes both commercially available software and shareware to be installed in order to run the FIP and BIP modules.

GAMMA (http://www.gamma-rs.ch/)
A license for Gamma software is commercially available under terms from Gamma Remote Sensing AG. A code version of the gamma software is licenced by MDA for development use by R&D. The Gamma source provides well documented low-level methods for processing InSAR data and has become a standard code base for researchers globally. GAMMA has many modules for registering and resampling

stacks of imagery, interferogram generation, spatial coherence computation, baseline adjustment, phase unwrapping, and other operations.

xv (http://www.trilon.com/xv/)
This is a Linux visualization tool for X Windows Systems, available as shareware for individual use and commercially licensed for professional use. Xv can operate on images in GIF, JPEG, TIFF, Sun Rasterfile, BMP and other image format on all known types of X displays.

gdal (http://www.gdal.org/)
Image file format support is provided by the open-source GDAL (Geospatial Data Abstraction Library) raster geospatial data formats library. The library core is implemented in C/C++, but it also provides a Python interface. GDAL supports many formats, including GeoTIFF, RADARSAT-2, various flavours of CEOS, ENVISAT, TerraSAR-X, and many more. GDAL is a multi-platform library, supporting Linux, Windows, MacOS X, and Solaris. GDAL is part of the Open Source Geospatial Foundation (OSGeo).

A2 Data Interfaces

A description of the purpose, inputs and outputs for each FIP module is provided below where Table A-1 defines the characteristics of each file type and Table A-2 defines the number of bytes per pixel for each data type. All dates are expressed in YYYYMMDD format where YYYY represents the four-digit year, MM the two-digit month and DD the two-digit day.

Table A-1 File Type Descriptions

File Type	File Type	Description
atmospheric phase screens (*.atm)	Float	Binary file of atmospheric phase screen value (one file per interferogram). Naming convention is same as for interferograms (date1_date2.atm).
baseline files (*.base)	ASCII	Stores initial and precision baselines (one file per interferogram, GAMMA format). Naming convention same as for interferograms (date1_date2.base).
coherence files (*.cc)	Float	Binary file of spatial coherence, naming convention same as for interferograms (date1_date2.cc).
Deformation files (*.def)	Float	Binary file of deformation in metres. Naming convention is date.def, where date is in YYYYMMDD format.
DEM files	Float	Binary file with elevations measured with respect to the WGS84 ellipsoid. Horizontal datum can be geographic (i.e., latitude/longitude) or UTM.
gc_fine	Float complex	Geocoding table relating the map geometry to the radar geometry. Each pixel contains the corresponding range (real part) and azimuth (complex part) pixel locations in the radar image.
intensity images RMLI (*.rmli)	Float	Binary file of a registered multi-look intensity image (RMLI). Naming convention is date.rmli, where date is in YYYYMMDD format.

File Type	File Type	Description
interferograms (*.diff)	Float complex	Binary file, naming convention is date1_date2.diff, (date1 is master date, date2 is slave date).
itab	ASCII	List of interferogram combinations. Column 1 is the master index, column 2 is the slave index, column 3 and 4 are dummy columns (GAMMA format).
Masks	Byte	Store information about which pixels to process for different parts of the processing chain.
parameter files (*.par)	ASCII	Stores all metadata and parameters (e.g. image acquisition time, centre latitude/longitude, incidence angle, number of pixels, etc.). (GAMMA format)
pt (point) file	Long	Binary file of point locations (in pixels), stored in 2-column format of [rg,az]
pt latlon file	Float	Binary file of point locations (in degrees) stored in 2-column format of [lat,lon]
RMLI intensity images (*.rmli)	Float	Binary file of a registered multi-look intensity image (RMLI). Naming convention is date.rmli, where date is in YYYYMMDD format.
RSLC images (*.rslc)	Float complex	Binary file of a registered single look complex SAR image. Naming convention is date.rslc, where date is in YYYYMMDD format.
RSLC_tab	ASCII	List of locations of each RSLC image (column 1) and RSLC parameter file (column 2) in the stack.
spectral diversity (*.sp_cc)	Float	Spectral diversity files (one file per scene). Naming is date.sp_cc where date is in YYYYMMDD format.
temperature file	ASCII	List of temperatures for each acquisitions. Column 1: acquisition date in YYYYMMDD format, column 2: temperature in degrees Celsius.

Table A-2 Interface file types with corresponding bytes per pixel

File Type	Bytes per Pixel
Byte	1
Long	4
Float	4
Float Complex	8
Double	8

active_layer.pro:

purpose: create an active layer deformation template function using temperature time series data based on LIU's 2012 paper on estimating active layer thickness.

inputs: temperature text file in the format of "YYYYMMDD TEMP " per line and a temperature offset estimating the air to ground temperature difference.

outputs: Text file containing the active layer template in the format "YYYYMMDD AL_VALUE".

gen_svd_residuals.pro:

purpose: create unwrapping error residuals and spatial + temporal maps of these residuals.

inputs: unwrapped interferograms and SVD inverted phase results + metadata

outputs: residual maps per network layer and spatial + temporal maps of these residuals.

gen_svd_residuals_pt.pro:

purpose: point based wrapper to gen_svd_residuals.pro

inputs: additional input of pt file.

outputs: see gen_svd_residuals.pro

hds_filt_phase_deramp.pro:

purpose: Filter input data (float or complex) according to HDS neighbourhoods using deramping method

inputs: itab, RSLC_tab, interferograms, HDS probability map (from mk_hds_neigh.pro), etc.

outputs: network of filtered HDS interferograms *.diff.natm.hds

hds_filt_phase_deramp_render.pro:

purpose: Render data including debug data for the deramping.

inputs: hardcoded.

outputs: debug imagery

phase_deramp_testbed.pro:

purpose: estimate spatial slope of topographic error and linear deformation (point click version)

inputs: itab, RSLC_tab, interferograms, HDS probability map (from mk_hds_neigh.pro), etc.

output: interactive debugging viewer into deramping algorithm

transect__define.pro:

purpose: Class handling transect definition and data extraction

inputs: KML file or mask defining transects, io and transform instances

output: instance of a transect class for transect based operations

interp3d.pro:

purpose: interpolation along a 3D curve

inputs: x, y, and z inputs of curve and t defining normalized interpolation points along curve.

output: interpolated 3D curve

is_within_polygon.pro:

purpose: determine if points fall within polygon

inputs: list of points to check, polygon definition

output: byte array signalling which points were within (1) and which were outside (0).

mia_demod_unw.pro:

purpose: convenience wrapper that allows for running unwrapper on multiple stacks

inputs: see configuration file

output: unwrapped phase stack for each beam being MIA processed

mia_hgt_defmod_remove.pro:

purpose: convenience wrapper that allows for running model corrections on multiple stacks

inputs: see configuration file

output: corrected interferogram network

mia_merge_neigh.pro:

purpose: merge neighbourhoods from each of the independent stacks into one joint result.

inputs: neighbourhoods from each stack

output: merged neighbourhood and probability files

mia_mk_diff.pro:

purpose: Generate interferograms for all stacks in the master geometry

inputs: see configuration file

output: interferograms for all stacks in the master geometry

mia_mk_hds_neigh.pro:

purpose: generate the joint neighbourhoods from all stacks (makes use of mia_merge_neigh.pro)

inputs: see configuration file

output: merged neighbourhood and probability files

mia_remap.pro:

purpose: script to remap data from slave to master geometry

inputs: see configuration file

output: remapped data

mia_remap_glob.pro:

purpose: convenience wrapper around mia_remap to remap multiple files via glob patterns

inputs: see configuration in source

output: remapped data

mia_remap_make_par.pro:

purpose: generate gamma par file for MIA master/slave geometries

inputs: slave/master par files

output: mia slave/master par files

mia_remap_subset.pro:

purpose: determine subset bounds of master scene in slave geometry

inputs: subset definition of master and slave to calculate for.

output: subset bounds in slave geometry

mia_remap_table.pro:

purpose: generate remapping table from slave to master geometry

inputs: see configuration file.

output: remapping lookup table from slave to master

mia_subset.pro:

purpose: run subsetting tools for all slave stacks mapping data to master geometry.

inputs: see configuration file

output: MIA directory containing the master subset and all corresponding slave data for Multi-Track HDS processing

A3 Data Flow

The sections below list the sequence of commands for running the FIP described in Section A2. It is assumed that all hardware and software requirements detailed in Section **Error! Reference source not found.** have been met and that the MDA-rovided compiled IDL file mda_rnd_imp_bip.sav is on the user's path, copied in the active directory or symbolically linked to the user's active directory.

The first time running most routines within a given directory, a new configuration (.cfg) file will be generated that the user must edit with their favourite editor. Save and close the .cfg file and re-run the same IDL command to execute the program. Note that due to the use of compiled BIP modules, all routines must be run in single-threaded mode, such that the variable single_thread should always be set to 1.

A3.1 List of available tools

The following tables shows all available commands in the bip file – to run any first the .sav file must be loaded:

Load compiled IDL modules:

```
IDL> restore, 'mda_rnd_imp_bip.sav'
```

Table A-3 lists the sequence of commands for the full scene processing which must be performed first. Table A-4 lists the subset region processing commands (denoted MIA-HDS commands) which are run after full scene processing is complete). All scripts will generate a configuration file that must be edited. A master configuration file can be generated with the python script gen_master_cfg.py. This is used for convenience in all subsequent configuration files as it is read and fills in any master configuration tags. Note that some of these will require data generated via GAMMA software tools.

Table A-3 Full Scene Processing Overview

Commands	Description
dem_hilo_blend	If hi-res DEM available merge it to lo-res SRTM DEM just obtained or other DEM (e.g. Geobase, USGS)
dem2rdc_ratfun	Calculate mapping from geo coordinates (EQA/UTM) to RDC coordinates and project DEMs to RDC
mk_diff	Calculate course resolution differential interferograms
base_opt	Baseline optimization of network using coherence maximization
mk_atm_corr2d	Generate long-range atmospheric phase screens

Table A-4 MIA-HDS Processing Overview

Program/Script	Description
mia_subset	Generate MIA processing directory and generate slave stack subsets + remapping tables and remap slaves to master geometry
mia_mk_diff	Generate interferograms for master and slave stacks and remap the slave interferograms to the master geometry
mia_mk_hds_neigh	Identify HDS neighbourhoods in all stacks and create joint results for MIA processing
mk_diff_coh_all	Calculate the joint temporal differential coherence
hgt_defmod_corr_peaksmth	Estimate the joint peak-to-peak differential coherence
hgt_defmod_corr_peaksmth	Estimate the joint residual height error, linear deformation, and/or thermal dilation
qual_thresh	Generate renderings to interactively determine best quality threshold
pt_select	Select HDS points using quality threshold and extract complex data and phase models at the select locations for all stacks
mia_demod_unw	Unwrap each interferogram in network in all stacks
mk_svd_invert_pt	Invert network of phase using SVD to derive joint time series of phase
svd2totaldef_pt	Temporally filter joint time series
view_trace	View temporal traces of select points

Additional helpers are available and can be viewed via the IDL help command, though the above listed commands represent the top level processing calls.